

1 Marine intrusions in a microtidal coastal lagoon and their influence on the entry  
2 of meroplankton

3

4 Irene Machado<sup>1\*</sup>, Lorena Rodríguez-Gallego<sup>1</sup>, Magda C. Sousa<sup>2</sup>, Danilo Calliari<sup>3</sup>,  
5 Américo Ribeiro<sup>2</sup>, João Pedro Pinheiro<sup>2</sup>, Daniel Conde<sup>4</sup>, João Miguel Dias<sup>2</sup>

6 1 Departamento Interdisciplinario de Sistemas Costeros y Marinos, Centro Universitario  
7 Regional Este, Universidad de la República, Ruta 9 km 206, CP 27000, Rocha, Uruguay

8 2 CESAM, Physics Department, University of Aveiro, Aveiro 3810-193, Portugal

9 3 Sección Oceanografía y Ecología Marina, Instituto de Ecología y Ciencias  
10 Ambientales, Facultad de Ciencias, Universidad de la República, Iguá 4225,  
11 Montevideo, Uruguay

12 4 Sección Limnología, Instituto de Ecología y Ciencias Ambientales, Facultad de  
13 Ciencias, Universidad de la República, Iguá 4225, Montevideo, Uruguay

14

15 \*Corresponding author Irene Machado, e-mail: [imachado@cure.edu.uy](mailto:imachado@cure.edu.uy)

16

17 **Abstract**

18 It is essential for the functioning of intermittently closed/open lagoons and lakes (ICOLLs)  
19 to maintain a connection with the adjacent sea. This connectivity allows larval stages,  
20 like planktonic larvae, of marine estuarine-related species to move between  
21 environments by relying on water flows when the sandbar is open. This study aims to  
22 research the dynamics of marine intrusions into a microtidal coastal lagoon - Laguna de  
23 Rocha, Uruguay as a case study - during the open state of the sandbar. A 2-D  
24 hydrodynamic model was constructed, and model results were calibrated and validated  
25 with *in situ* data. A seawater tracer was used to determine the frequency, duration and  
26 intensity of marine intrusion under different wind, sea level and tributary discharge  
27 scenarios. Results showed that under calm conditions (light wind and basal discharge)  
28 at least one marine intrusion per day occurred in the vicinity of the inlet channel due to  
29 high tide. The sea level was essentially the main determinant of the duration of marine  
30 intrusions. Sea level rise has led to an increase in the duration (up to 22 hours per day)  
31 and spatial extent of marine intrusions. Conversely, tributary discharge primarily  
32 determined the intensity of marine intrusions attenuating them under high discharge

ICOLLs: intermittently closed/open lagoons and lakes  
LR: Laguna de Rocha

33 scenarios. Strong SE (onshore) winds increased the duration of marine intrusions in all  
34 scenarios and the intensity of intrusions in the low sea level scenarios. Results about the  
35 importance of sea level for marine intrusions in Laguna de Rocha broaden the possible  
36 mechanism by which meroplankton can enter these microtidal systems. For instance, it  
37 could involve a combination of forces that overlap to raise the sea level above the lagoon  
38 water level (e.g. onshore winds, spring tides). Results suggest that the main force  
39 triggering seawater and larval entry may vary over time in the same lagoon. Therefore,  
40 in the microtidal Laguna de Rocha, we propose a mechanism for selecting incoming  
41 currents for the entry of estuarine-related larvae that, unlike other proposed mechanisms,  
42 may not be solely due to the effect of flood tide.

43

44 Keywords: hydrodynamic model; Delft3D; ICOLL; estuarine-dependent species;  
45 meroplankton; Laguna de Rocha

46

## 47 **1 Introduction**

48 The connectivity between estuaries and the adjacent sea is relevant for the ecological  
49 functioning of both ecosystems. The exchange of water between the sea and estuaries  
50 is influenced by factors such as tributary discharge, tidal amplitude, wind action and  
51 geomorphology (Valle-Levinson 2010). In meso- to macro tidal environments, tidal  
52 currents play a significant role on hydrodynamics (Dias et al. 2021), generating seawater,  
53 macromolecules and organisms of marine origin inflows, while low tides export these  
54 elements of fluvial and terrestrial origin from the estuaries to the sea (Amaral et al. 2020).  
55 In meso- to microtidal estuaries, wind and tributary discharge are more influential,  
56 affecting the hydrodynamics and organisms of these systems (Martins et al. 2007, Bruno  
57 and Acha 2015, Tuchkovenko et al. 2019). Coastal lagoons belonging to intermittently  
58 closed/open lagoons and lakes type (ICOLLs) (Roy et al. 2001) are environments that  
59 typically originate in mid-latitudes where the tidal range is low, and wave action allows a  
60 sandbar to form along the coast (Mc Sweeney et al. 2017). Seawater intrusion into these  
61 environments also depends on the morphology of the lagoons and the channel  
62 connecting them to the sea (Fiandrino et al. 2017, Tuchkovenko et al. 2019).

63 Some species in coastal lagoons are estuarine-dependent or opportunistic species,  
64 including croakers (e.g. *Micropogonias furnieri*), mullets (e.g. *Mugil lisa*) and shrimps  
65 (e.g. *Penaeus paulensis*), which are of economic importance (e.g. Fabiano and Santana  
66 2006). Similarly, some crabs, such as the blue crab (e.g. *Callinectes sapidus*) or the

67 burrowing crab (e.g. *Neohelice granulata*), play an essential role as target species for  
68 fishing or as ecosystem engineers due to their role of bioturbation in the sediments, and  
69 have larval export strategies (Bas et al. 2009, Epifanio 2019). These species need to  
70 enter the estuary during their larval stage (estuarine-related), and it is therefore essential  
71 to know the potential mechanisms involved. It is known that larvae are planktonic and  
72 that their swimming ability is limited, so they must develop strategies that allow them to  
73 take advantage of currents to move between environments (Joyeux 1998, Pineda et al.  
74 2007). The combined influence of physical and behavioural factors determines the  
75 transport of larvae from breeding to nursery areas (Tankersley 2001, Queiroga and  
76 Blanton 2005). The success of the transport during the larval stage is largely dependent  
77 on the correct coupling of these factors (Iles and Sinclair 1982, Pineda et al. 2007).

78 The process by which larvae adapt their behaviour to tidal currents has been extensively  
79 studied and has been termed selective tidal stream transport (STST) (e.g. Tankersley  
80 2001). Several studies showed the importance of tidal currents for the entry of larval  
81 stages of estuarine-dependent species of shrimp (Ogburn et al. 2013) and fish (Jager  
82 1999, Hale and Targett 2018) or for the re-entry of crab larvae with larval export strategy  
83 (Queiroga et al. 2006, Epifanio 2019). The effect of wind on sea level and circulation can  
84 modulate the impact of STST and influence larval transport, particularly in coastal  
85 lagoons (Joyeux 1998, Queiroga et al. 2006). In addition, a combination of tidal and wind  
86 intensity has been observed as a driving force for the entry of estuarine-dependent larvae  
87 in a microtidal lagoon estuary (Bruno and Acha 2015, Bruno et al. 2018). Conversely,  
88 prolonged periods of intense rainfall have been shown to impede the recruitment of  
89 estuarine-dependent species in other microtidal coastal lagoon (Möller et al. 2009).

90 Due to the high variability of the forcings, field studies to determine the mechanisms of  
91 larvae movements into and out of coastal lagoons are usually very complex to  
92 implement. It is required a significant sampling effort both spatially and temporally, and  
93 some key processes may not be represented as those during storms. Considering these  
94 limitations, hydrodynamic modelling is a powerful and effective tool for understanding  
95 complex spatio-temporal processes that require high spatial and temporal resolution, to  
96 adequately follow the effects of poorly predictable forcing (e.g. non-astronomical forcing).  
97 This type of tool has been used to determine larval transport to breeding areas (Martins  
98 et al. 2007, Dickey-Collas et al. 2009). For example, the importance of wind direction  
99 and intensity on larval circulation and transport has been highlighted (Simionato et al.  
100 2008, Franzen et al. 2019). Similarly, modelling can be utilized to simulate various  
101 scenarios and observe how different forcings change estuarine hydrodynamics or larval  
102 transport (Martins et al. 2007, Simionato et al. 2008, Dias et al. 2021).

103 Despite previous studies in microtidal estuaries and particularly in coastal lagoons (e.g.  
104 Whitfield et al. 2023), there are still unanswered questions regarding the entry of  
105 estuarine-related species larvae: i) How frequently do marine intrusions that enable the  
106 entry of larvae occur? ii) What are the duration and intensity of these intrusions? iii) How  
107 do sea level, tributary discharge and wind influence the duration and intensity of marine  
108 intrusions? iv) What is the spatial extent of the impact of the intrusions?

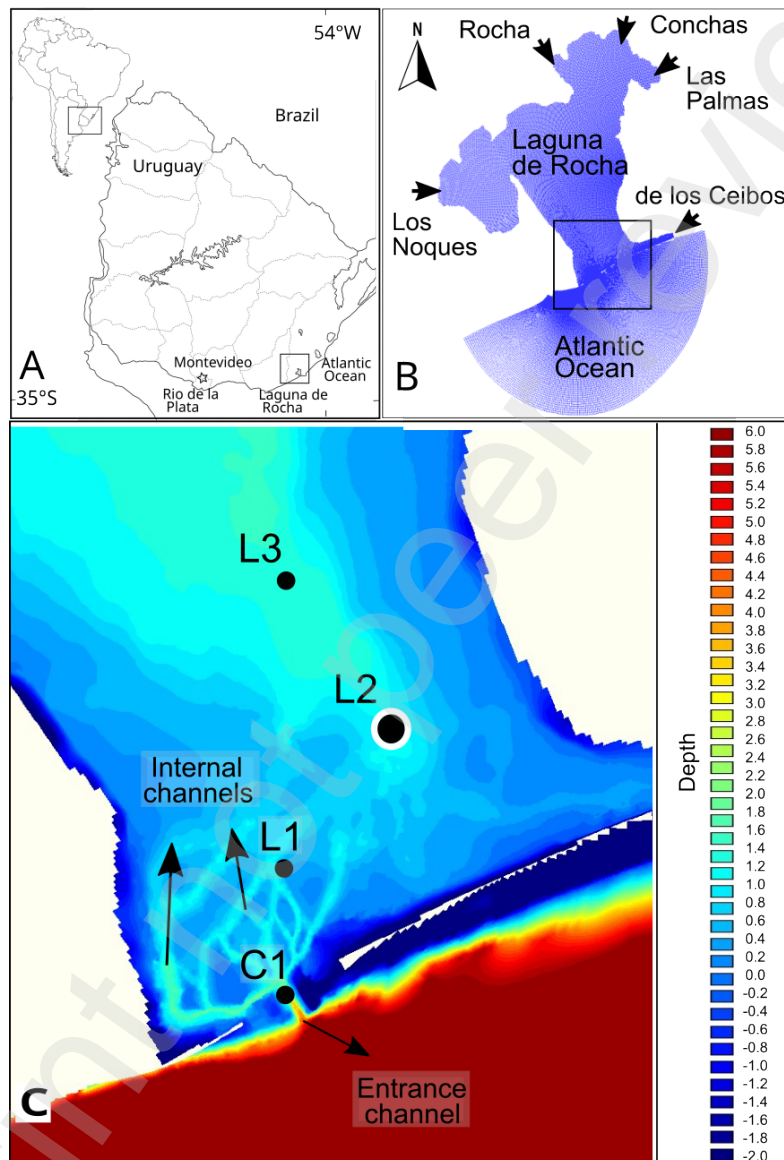
109 This study aims to understand the marine intrusions into a coastal lagoon, using  
110 hydrodynamic modelling to answer the abovementioned questions in Laguna de Rocha  
111 (Uruguay). A 2-D hydrodynamic model (Delft3D) was implemented, and *in situ* data was  
112 used to calibrate and validate the model and interpreted the results. Then, several  
113 numerical simulations were carried out to include scenarios that could occur based on  
114 the combination of different climatic and hydrological drivers, using the FLOW module of  
115 Delft3D. These simulations have enabled the analysis of the inflow of seawater under a  
116 variety of environmental conditions. Finally, the mechanisms through which estuarine-  
117 related meroplankton larvae gain access to estuaries, as well as the inherent natural  
118 challenges posed by climatological variations were discussed.

## 119 **2 Study area**

120 Laguna de Rocha (LR) and the adjacent coastal waters (CW) are located on the  
121 Southwestern Atlantic Ocean coast (34° 38' S - 54° 17' W, Uruguay, Fig. 1). This area is  
122 characterised by a subtropical climate with maximum air temperature in summer  
123 (average = 21°C) and minimum in winter (average = 11°C) (Barreiro et al. 2019). The  
124 region exhibits two semidiurnal tides with diurnal inequalities, the main one being the M<sub>2</sub>  
125 (main semidiurnal lunar component) accounting for 65% of the total tidal energy  
126 (D'Onofrio et al. 1999). The tidal range is about 40 cm, categorizing it as microtidal.  
127 However, atmospheric disturbances, particularly from wind, often surpass astronomical  
128 effects, resulting in sea level variations of up to 3 m above the expected astronomical  
129 tide (Alonso et al. 2017). Sea level variations on the Patagonian shelf are crucial in  
130 determining sea level changes in Uruguayan marine and estuarine waters, where the  
131 signal can be amplified or reduced by local conditions (Alonso et al. 2017). On the coast  
132 of Uruguay, NE winds are predominant year-round and are more frequent in spring and  
133 summer, leading to the generation of upwelling in these seasons (Piola et al. 2008, de  
134 Mello et al. 2022). East winds are also significant (Manta 2017). At the same time, the  
135 dynamics of the sea breeze, an air circulation generated by the differential heating  
136 between land and sea, are essential in the study area. Generally, the sea breeze starts  
137 at 11:00 on the seacoast, has a southeast direction and reaches a maximum speed of

138 7.1 m s<sup>-1</sup> around 16:00 (Manta et al. 2021). This phenomenon is more frequent in  
139 summer. Precipitation in the study area is 1122 mm per year, showing no seasonal  
140 variations (Uruguayan Institute of Meteorology [INUMET]), although evapotranspiration  
141 is highly seasonal.

142



143

144 Figure 1. A) Location of the study area on the Atlantic coast of Uruguay. B) Irregular  
145 curvilinear grid used for the hydrodynamic modelling of the Rocha Lagoon and the  
146 adjacent sea. The black arrows indicate the location of the five tributary discharge sites  
147 included in the model. The curved area indicates the open oceanic boundary. C) Detail  
148 of the bathymetry of the channel area (colour gradient) and location of the model grid  
149 cells where the model output data were observed (black circles) and of the buoy where  
150 the field sensors were anchored (white circle).

151

152 LR is a very shallow lagoon with a mean depth of 0.6 m. The lagoon covers an area of  
153 72 km<sup>2</sup> and has a catchment area of 1214 km<sup>2</sup> with an intermittent connection to the sea  
154 (ICOLL type according to Roy et al. 2001) (Fig. 1). The average daily flow received by  
155 the lagoon from its tributaries is 17.7 m<sup>3</sup> s<sup>-1</sup>. The connection to the sea is through a  
156 channel that opens over the sand barrier (Rodríguez-Gallego et al. 2017). When LR is  
157 disconnected from the sea, the discharges of the tributaries raise the water level inside  
158 the lagoon until the sandbar breaks and a channel is established, which can last several  
159 months. After lagoon discharge, a seawater intrusion occurs, and the exchange  
160 continues as long as the channel remains open until the dynamics of sediment transport  
161 rebuild the sandbar (Conde et al. 2019). The inlet opens at least once a year, either  
162 naturally or artificially by the Municipality to reduce field floods and last several months.  
163 The exchange between the lagoon and the sea during the open sandbar period  
164 generates highly dynamic processes in the environment (e.g. of salinity and turbidity)  
165 and biological conditions within the lagoon (Rodríguez-Gallego et al. 2017; Espinosa et  
166 al. 2019, Machado et al. 2021).

167 LR and CW have been declared protected areas by Uruguayan national regulations and  
168 international conventions (e.g. Ramsar) due to their landscape value and the ecosystem  
169 services they provide. Some key species in these environments, such as the crabs *N.*  
170 *granulata* and *C. sapidus*, the shrimp *P. paulensis* and fish such as *M. furnieri*,  
171 *Symphurus plagiusa* (tonguefish) and *Paralichthys orbignyanus* (flounder), are  
172 estuarine-dependent or opportunistic species. These species move between the sea and  
173 the lagoon, generally entering at advanced larval stages and eventually recruiting into  
174 the lagoon (Santana et al. 2015, Machado et al. 2021). Although the entry of these larvae  
175 through overwash events has been observed, the exchange is usually more significant  
176 during the open sandbar state (Machado et al. 2021).

### 177 **3 Hydrodynamic model implementation**

#### 178 **3.1 Hydrodynamic model**

179 Delft3D-FLOW module is an open-source hydrodynamic modelling software developed  
180 by Deltares Institute in cooperation with Delft University of Technology. The model solves  
181 the baroclinic Navier-Stokes equation and the Boussinesq transport equation in 2D or  
182 3D. The FLOW module performs water level calculations. A detailed description of this  
183 model can be found in Lesser et al. (2004). A seawater tracer included in the FLOW  
184 module was used to assess the dynamics of seawater intrusion into LR under different  
185 forcing conditions. This Delft3D-FLOW module has been widely used in estuarine

186 systems in various regions, such as Portugal (e.g. Sousa et al., 2018), and Spain (e.g.  
 187 Carballo et al. 2009), among others.

### 188 **3.2 Model configuration**

189 The area used for the hydrodynamic calculations includes LR and CW and corresponds  
 190 to an open sandbar state (Fig. 1, Table 1). A two-dimensional model implementation was  
 191 developed to simulate the LR dynamics. The Delft3D-FLOW module was configured with  
 192 a curvilinear irregular grid (327 x 453 cells), with a resolution ranging from ~200 m at sea  
 193 and up to ~9 - 30 m in the channel zone connecting the lagoon and the ocean. Within  
 194 the lagoon, resolution gradually increases to 120 m in the north of the lagoon and at the  
 195 open sea boundary (Fig. 1 B). The numerical bathymetry assumes an open sandbar  
 196 state and that the shape of the channel does not change with time. The model  
 197 configurations developed consider that the fluid is Newtonian, and that its density is  
 198 constant. Bottom roughness was assumed to be uniform over the study area and not  
 199 time-varying. Viscosity and horizontal eddy diffusivity were assumed to be constant. The  
 200 model was implemented with open boundary conditions from September to October  
 201 2016. The first month was considered as the time when the model reached equilibrium  
 202 (spin-up) and the variables were balanced. Table 1 summarises the main features of the  
 203 simulation, including resolution and parameterisations.

204

205 Table 1. Main characteristics and parameters used in the Delft3D numerical simulations.

206

Parameter	Specification
Domain	54° 22' 00 "W to 54° 10' 00 "W 34° 32' 00 "S to 34° 50' 00 "S
Resolution	~200 m in the sea, ~9 – 30 m in the inlet between the lagoon and sea, increasing gradually to 120 m in the north of the lagoon
Gravity	9,81 m s <sup>-2</sup>
Water and air density	1000 kg m <sup>-3</sup> and 1 kg m <sup>-3</sup>
Oceanic boundary Forcing	Hourly water level
Transport condition	Water level
Discharge	Daily discharge of 5 streams, calculations based on measured rainfall in the study area
Bottom roughness	Constant Manning's roughness coefficient of 0.024 Chezy formula with 500 to 4000 µm sediment diameters
Horizontal eddy Viscosity	0.5 m <sup>2</sup> s <sup>-1</sup>
Horizontal Eddy Diffusivity	10 m <sup>2</sup> s <sup>-1</sup>
Wind	Hourly data from station located on the coast, 40 km from the study area
Time period	01/08/16 to 31/10/16
Time step	15 seconds

207

208

209 The bathymetry of the entire area was assembled from different sets of available data  
210 taken at different times, including the lagoon body, the inundation area, and the channel  
211 area connecting the sea, the lagoon, and the coastal area. Most of the data comes from  
212 measurements obtained by the Universidad de la República and the Uruguayan National  
213 Navy (e.g. nautical charts). To assign a bathymetric value to each grid node, the  
214 averaging function and the triangular interpolation function were used first. Several  
215 bathymetries were carried out, considering the different shapes of the access channel  
216 (depth and width) and the internal channels of the estuary, using satellite images of the  
217 study area (using true colour analysis, RGB) as a guide. The different bathymetries were  
218 part of the model calibration adjustments.

219 Thirteen main tidal harmonic constants ( $M_2$ ,  $S_2$ ,  $N_2$ ,  $K_2$ ,  $K_1$ ,  $O_1$ ,  $P_1$ ,  $Q_1$ ,  $M_{sf}$ ,  $M_m$ ,  $M_4$ ,  $MS_4$   
220 and  $MN_4$ ) from global data from the TPXO 7.2 TOPEX/Poseidon Altimetry model  
221 (<http://volkov.oce.orst.edu/tides/global>), with a spatial resolution of ~25 km, were used as  
222 astronomical forcing at the oceanic open boundary. In addition, hourly sea level data for  
223 the study area were obtained from the Copernicus Global Reanalysis (PHY\_001\_024)  
224 (<https://resources.marine.copernicus.eu/products>). The sea level corresponding to the  
225 sum of the astronomical tidal amplitude (calculated based on harmonics) and the sea  
226 level amplitude obtained from the Copernicus sea level base was used, which correctly  
227 described the data observed *in situ* at the port of La Paloma (SHOMA), located 13 km to  
228 the east of the lagoon mouth.

229 The location of the discharges was defined according to the main tributaries of LR, four  
230 in the north of the lagoon and one in the southeast (Fig. 1 B). Daily discharge estimates  
231 ( $m^3 s^{-1}$ ) generated by IMFIA-UdelaR using the GR4J model (Perrin et al. 2003), adapted  
232 for Uruguay (Narbondo et al. 2020), were used. This model was based on rainfall and  
233 potential evapotranspiration data obtained from the INUMET Rocha meteorological  
234 station, located 20 km from the study area, within LR watershed. The most significant  
235 discharge to the lagoon is from Rocha (60% of the total tributary discharge), followed by  
236 Las Conchas (17.5%), Las Palmas (10%), and Los Noques streams (9.4%), and De los  
237 Ceibos creek (3.1%) (Rodó 2013).

238 Surface boundary conditions were established using hourly wind data from a coastal  
239 weather station near the study area located in José Ignacio, approximately 40 km away  
240 (Manta et al. 2021). Spatially uniform wind was considered.

241 The model was calibrated by adjusting the bottom friction coefficient, the viscosity and  
242 the bathymetry of the internal channels connecting the main channel and the centre of  
243 the lagoon (Fig. 1 C). Bottom roughness was assumed to be uniform over the study area

244 and without temporal variation. Several simulations were carried out varying the bottom  
245 roughness, on the one hand using the Manning coefficient (0.024, for  $u$  and  $v$ ) and, on  
246 the other hand, changing the mean sediment grain size in the Chezy coefficient between  
247 500 and 4000  $\mu\text{m}$ .

248 The model validation was performed by comparing the temporal evolution of the  
249 simulated water level inside the lagoon at L2 and the data measured *in situ* with a tide  
250 gauge (EMAC-IADO) located at the same site (Fig. 1 B) during September 2016. Due to  
251 an existing referencing problem of the lagoon level data measured *in situ*, the data were  
252 compared by removing the mean (RM). To determine the performance of each model  
253 configuration on the water level in the lagoon, the root mean square error (RMSE) and  
254 its associated error (Skill) were estimated (Dias et al. 2009). RMSE and Skill can have  
255 values between 0 and 1; an RMSE of 0 and a Skill of 1 represents an excellent  
256 agreement between the model results and observed surface elevation.

257

### 258 **3.3 Marine intrusion scenarios**

259 The frequency, duration and intensity of marine intrusions under different environmental  
260 conditions or scenarios were studied for spring, the main period when larvae of  
261 estuarine-related species enter the lagoon. Ten days of unchanged conditions (wind,  
262 tributary discharge, and sea level) were used for training (spin-up), and then the  
263 conditions were adjusted according to the proposed scenarios for three days (72 h). The  
264 entry of seawater into the lagoon (a necessary condition for the entry of planktonic  
265 larvae) was evaluated by monitoring a seawater tracer simulating neutral particles  
266 (density  $1000 \text{ kg m}^{-3}$ ), with an arbitrary initial concentration in the sea of  $1 \text{ kg m}^{-3}$ . The  
267 concentration of the tracer was estimated in the entrance channel (C1) and at three sites  
268 within the lagoon (L1, L2 and L3), located at increasing distances from the main channel  
269 (approximately 0.5, 1.5 and 3 km) (Fig. 1 C). The Delft3D-FLOW module was also used  
270 for tracer tracking. A total of 30 scenarios were analysed. The construction of these  
271 scenarios involved the combination of the three forcings (factors) with the most  
272 significant expected effect on the hydrodynamics of the system: wind (five conditions),  
273 tributary discharge (two conditions) and sea level (three conditions).

274 For wind, the five conditions considered were the most frequent combinations of direction  
275 and intensity in the study area during spring and the breeze cycle (Manta 2017) (Table  
276 2). The two discharge conditions were defined based on the study of total estimated  
277 discharges (from 1983 to 2017) in LR during spring (Narbondo et al. 2020). Based on  
278 these criteria, a basal and high discharge corresponding to the 50 and 95- percentile

279 were selected, defined as  $5 \text{ m}^3 \text{ s}^{-1}$  and  $75 \text{ m}^3 \text{ s}^{-1}$ , respectively. Based on the analysis of  
 280 the water level boundary conditions in the adjacent coast during spring 2016, three  
 281 periods with different sea level were selected: a low period (from 2 to 4 October), a  
 282 medium period (from 21 to 23 October), and a high period (15-17 November),  
 283 characterized by a mean sea level of -0.1, 0.1 and 0.3 m, respectively. Table 2  
 284 summarises the proposed scenarios ( $n = 5 \times 2 \times 3 = 30$ ).

285

286 Table 2. Scenarios ( $n=30$ ) to evaluate the duration and intensity of marine intrusions  
 287 using a tracer. The table shows the three forcings with their respective categories: 1)  
 288 wind ( $\text{m s}^{-1}$ ): 5 categories, four fixed and one variable. 2) sea level (m): 3 categories. 3)  
 289 tributary discharge ( $\text{m}^3 \text{ s}^{-1}$ ): 2 categories.

Wind ( $\text{m s}^{-1}$ , degree)		Low Sea Level (LSL: average= -0.3 m)		Medium Sea Level (MSL: average= -0.1 m)		High Sea Level (HSL: average= 0.1 m)	
FIXED	Light NE (S-NE: $2 \text{ m s}^{-1}$ , 45 degree)	Basal discharge ( $5 \text{ m}^3 \text{ s}^{-1}$ )	High discharge ( $75 \text{ m}^3 \text{ s}^{-1}$ )	Basal discharge ( $5 \text{ m}^3 \text{ s}^{-1}$ )	High discharge ( $75 \text{ m}^3 \text{ s}^{-1}$ )	Basal discharge ( $5 \text{ m}^3 \text{ s}^{-1}$ )	High discharge ( $75 \text{ m}^3 \text{ s}^{-1}$ )
	Moderate NE (M-NE: $6 \text{ m s}^{-1}$ , 45 degree)	Basal discharge ( $5 \text{ m}^3 \text{ s}^{-1}$ )	High discharge ( $75 \text{ m}^3 \text{ s}^{-1}$ )	Basal discharge ( $5 \text{ m}^3 \text{ s}^{-1}$ )	High discharge ( $75 \text{ m}^3 \text{ s}^{-1}$ )	Basal discharge ( $5 \text{ m}^3 \text{ s}^{-1}$ )	High discharge ( $75 \text{ m}^3 \text{ s}^{-1}$ )
	Moderate SEE (M-SEE: $6 \text{ m s}^{-1}$ , 129 degree)	Basal discharge ( $5 \text{ m}^3 \text{ s}^{-1}$ )	High discharge ( $75 \text{ m}^3 \text{ s}^{-1}$ )	Basal discharge ( $5 \text{ m}^3 \text{ s}^{-1}$ )	High discharge ( $75 \text{ m}^3 \text{ s}^{-1}$ )	Basal discharge ( $5 \text{ m}^3 \text{ s}^{-1}$ )	High discharge ( $75 \text{ m}^3 \text{ s}^{-1}$ )
	Strong SE (F-SE: $12 \text{ m s}^{-1}$ , 135 degree)	Basal discharge ( $5 \text{ m}^3 \text{ s}^{-1}$ )	High discharge ( $75 \text{ m}^3 \text{ s}^{-1}$ )	Basal discharge ( $5 \text{ m}^3 \text{ s}^{-1}$ )	High discharge ( $75 \text{ m}^3 \text{ s}^{-1}$ )	Basal discharge ( $5 \text{ m}^3 \text{ s}^{-1}$ )	High discharge ( $75 \text{ m}^3 \text{ s}^{-1}$ )
CHANGING	Sea breeze cycle (BM)	Basal discharge ( $5 \text{ m}^3 \text{ s}^{-1}$ )	High discharge ( $75 \text{ m}^3 \text{ s}^{-1}$ )	Basal discharge ( $5 \text{ m}^3 \text{ s}^{-1}$ )	High discharge ( $75 \text{ m}^3 \text{ s}^{-1}$ )	Basal discharge ( $5 \text{ m}^3 \text{ s}^{-1}$ )	High discharge ( $75 \text{ m}^3 \text{ s}^{-1}$ )

290

291

### 292 3.4 Marine intrusion assessment methodology

293 Marine intrusions into the lagoon in each scenario were characterised by number,  
 294 duration and intensity, estimated from changes in tracer concentration at the four model  
 295 observation sites (C1, L1 to L3). Marine intrusions were defined as periods when the  
 296 tracer concentration increased above threshold values. The thresholds were determined  
 297 as  $0.70$  and  $0.80 \text{ kg m}^{-3}$ , twice the baseline concentration in the calm scenarios (light

298 wind and no rain) corresponding to low and medium sea levels, respectively. The  
299 frequency was determined as the number of times the tracer exceeded these thresholds  
300 during the simulation period (72 h). The duration of intrusion was calculated by  
301 measuring the periods during which the tracer exceeded the predefined thresholds on  
302 each simulation day (24 h). The average peak widths over the three days were calculated  
303 (72 h). Intensity was calculated by averaging the maximum height of each simulation  
304 day. These daily averages are referred to as cases in the subsequent data analysis.

305 The sea level at the ocean boundary conditions was compared with the tracer  
306 concentration at the channel (C1). The time difference between the moment the  
307 maximum sea level peak occurs at the boundary (highest high tide) and the moment  
308 when the maximum tracer peak is recorded in the channel was determined. The  
309 relationship between the two variables was examined using the Spearman correlation.

310 Patterns in the duration and intensity of channel intrusions (site C1) and the importance  
311 of different forcings were determined using a Classification and Regression Tree (CART)  
312 model. CART models are easy to interpret and provide "yes or no" decisions on the  
313 thresholds of the main variables involved in branch divisions (e.g. De'ath and Fabricius  
314 2000). The CART was performed by dividing the cases (n=90, one per simulation day,  
315 i.e. 3 for each scenario) into 2/3 (n=60) and 1/3 (n=30), both for duration and intensity.  
316 The set with the highest number of cases was used to construct the models, using rpart  
317 v. 4.1.15 (Therneau et al. 2022) and partykit v. 1.2.6 (Hothorn and Zeileis 2015). A  
318 complexity coefficient (cp) of 0.001 and a minimum of 5 cases were considered before  
319 each partition to construct and build the trees. The resulting trees (one based on  
320 response duration and another based on intensity) were pruned according to the 1-SE  
321 rule, resulting in the tree with the best performance in terms of cost-complexity. The  
322 accuracy of the trees was evaluated using the set with the lowest number of cases (1/3).  
323 The number of misclassified cases divided by the total number of cases was used to  
324 calculate the error of each model. The final trees were presented graphically. All  
325 analyses were performed using R 3.5.3 (R Core Team 2019).

326

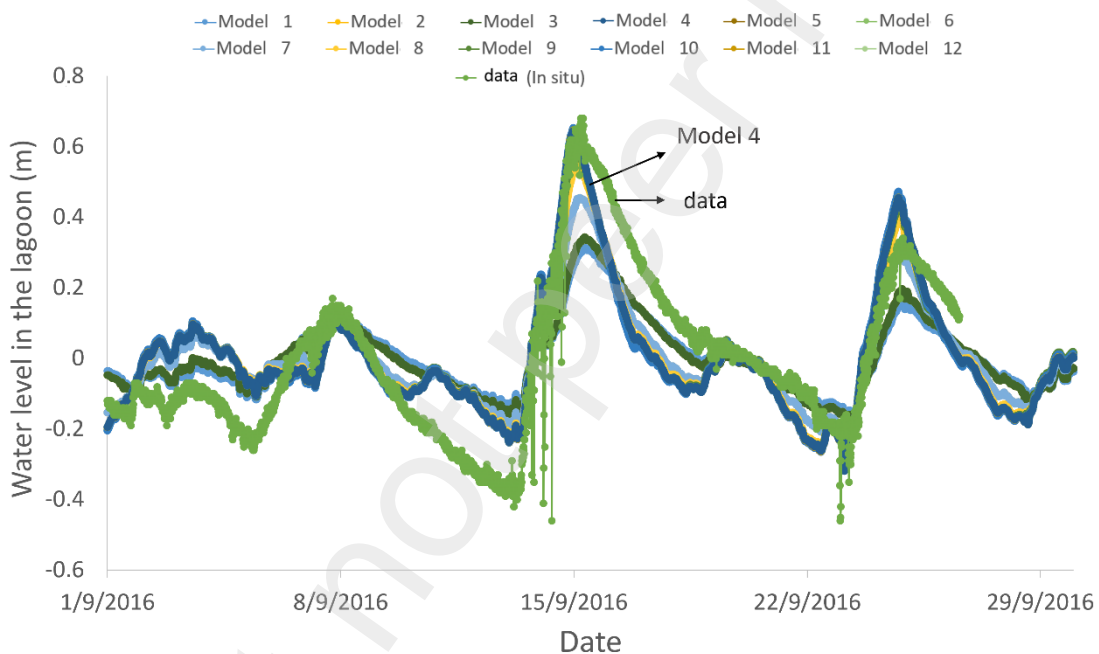
327 The extent, duration, and intensity of marine intrusions within the lagoon were compared  
328 in the four observation sites in the wind scenarios with the highest probabilities of  
329 occurrence: moderate SEE and strong SE. The average concentration and the deviation  
330 of the tracer during the three days of modelling in the study area were also determined.

331

332 **4 Results**

333 **4.1 Model validation**

334 The validation of the model was carried out with data from September 2016. During this  
335 period, the water level measured *in situ* showed three prominent peaks, and the  
336 maximum amplitude of the peaks recorded was 1.15 m (Fig. 2). The root mean square  
337 error (RMSE) between observations and model results ranged from 9.5 to 17.5% of the  
338 local amplitude, which means that the model performance can be classified from good  
339 to very good (Dias et al. 2009). The model configuration with the best performance was  
340 selected to simulate the dispersion of the tracer in marine waters (model 4, RMSE = 0.12  
341 m, skill of 0.90, Table 3).



342

343 Figure 2. Water levels measured in situ in the lagoon (buoy = L2) and those simulated  
344 by the different model configurations. The plot indicates the series corresponding to the  
345 in situ data (light green) and the model configuration with the best performance (dark  
346 green, Model 4).

347

348

349

350

351

352 Table 3. Summary of the configurations implemented in Delft3D, with the respective root  
353 mean square error (RMSE) and Skill. The model configuration selected for its best  
354 performance (model 4) is shown in bold.

355

Model code	Bottom roughness	Bathymetry	RMSE (m)	Skill
<b>Model 1</b>	Manning u, v=0.024	entrance channel, no internal channels at the mouth	0.12	0.83
<b>Model 2</b>	Manning u, v=0.024	entrance channel, with internal channels at the mouth	0.20	0.86
<b>Model 3</b>	Chezy SD <sub>50</sub> =3500μm	entrance channel, with internal channels at the mouth	0.12	0.86
<b>Model 4</b>	<b>Chezy SD<sub>50</sub>=500μm</b>	<b>entrance channel, With deep internal channels at the mouth overtopping</b>	<b>0.12</b>	<b>0.90</b>
<b>Model 5</b>	Chezy SD <sub>50</sub> =500μm	entrance channel, with internal channels at the mouth	0.11	0.89
<b>Model 6</b>	Chezy SD <sub>50</sub> =4000μm	entrance channel, with deep internal channels at the mouth	0.12	0.90
<b>Model 7</b>	Chezy SD <sub>50</sub> =3000μm	entrance channel, with internal channels at the mouth	0.11	0.89
<b>Model 8</b>	Chezy SD <sub>50</sub> =3500μm	entrance channel, with deep internal channels at the mouth	0.11	0.89
<b>Model 9</b>	Chezy SD <sub>50</sub> =3500μm	Deep entrance channel, with deep internal channels at the mouth	0.11	0.89
<b>Model 10</b>	Chezy SD <sub>50</sub> =3500μm	Deep entrance channel, with deep internal channels at the mouth overtopping	0.11	0.89
<b>Model 11</b>	Chezy SD <sub>50</sub> =3500μm	wide entrance channel, with internal channels at the mouth overtopping	0.12	0.90
<b>Model 12</b>	Chezy SD <sub>50</sub> =3500μm	wide entrance channel, with shallow internal channels at the mouth overtopping	0.12	0.90

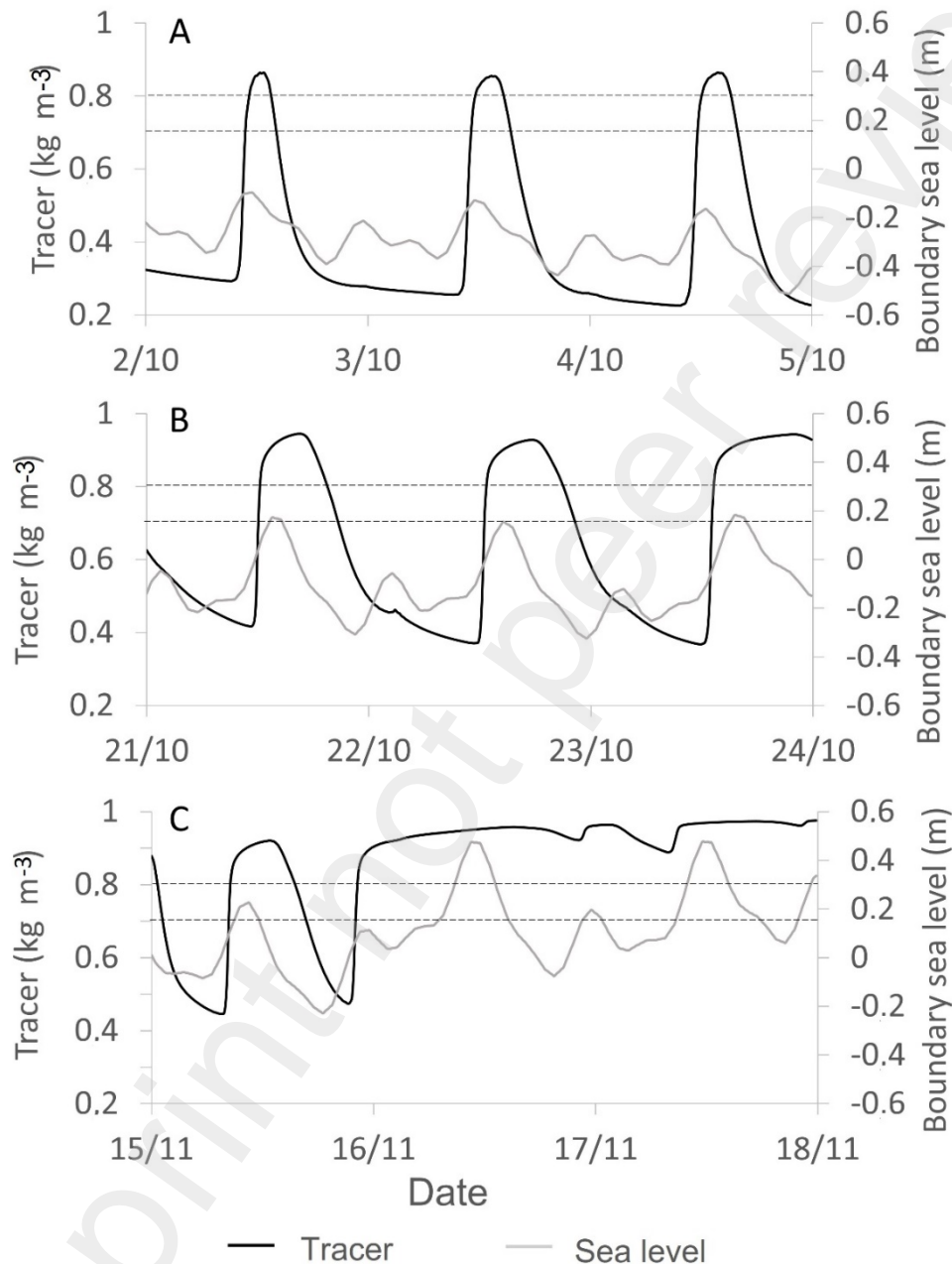
356

357

#### 358 **4.2 Number, duration, and intensity of marine intrusions under different conditions**

359 Three intrusion events were observed in the entrance channel under calm weather  
360 conditions (light wind and basal discharge) and low or medium sea level. These  
361 intrusions occurred every 24 hours. The concentration of the tracer was related to the  
362 variations in sea level in the boundary conditions (Spearman, rho=0.55 and 0.59;  
363 p<0.01), especially with the highest peak at high tide (Fig. 3 A and B). Under calm  
364 conditions and at high sea level (HSL), two intrusions were observed, and the  
365 concentration of the tracer showed a higher correlation with the sea level at the boundary  
366 compared to the other sea level scenarios (Spearman. rho=0.69; p<0.01). In this case,  
367 the daily lower peaks of water level also caused marine intrusions (Fig. 3 C). Intrusions  
368 in calm conditions had a longer mean duration with increasing sea level (from 3 to 18 h,  
369 Table 4). The intensity of marine intrusions was lower at low sea level (LSL) compared

370 to the other two sea level conditions (Table 4). The time difference between the highest  
 371 sea level peak at the ocean boundary and the peak of the tracer concentration in the  
 372 channel also increased with the mean sea level (1.4, 3.4 and 4 h respectively, Table 4).  
 373 These results indicate that even under calm conditions, there are daily inflows that can  
 374 be favourable for larval entry and that conditions improve with the increase in sea level.



375  
 376

377 Figure 3. Temporal variation of the tracer (left axis) in the entrance channel (C1) and of  
 378 the sea level at the sea boundary (right axis) under calm conditions (light NE wind and  
 379 basal discharge). A) low sea level. B) medium sea level and C) high sea level. The  
 380 horizontal lines indicate the 0.7 and 0.8 tracer thresholds.

381 Table 4. Comparison between tracer concentration and sea level at the ocean boundary  
 382 under calm conditions (light NE wind and basal discharge) for the three sea level  
 383 categories. The phase lag between the sea level peak at the boundary and the tracer  
 384 peak in the lagoon, the correlation between these two variables and the average width  
 385 and height  $\pm$  standard deviation of the peaks in the channel (C1) are indicated. LSL: low  
 386 sea level, MSL: medium sea level, HSL high sea level. \*: statistically significant  
 387 correlation ( $p < 0.01$ ).

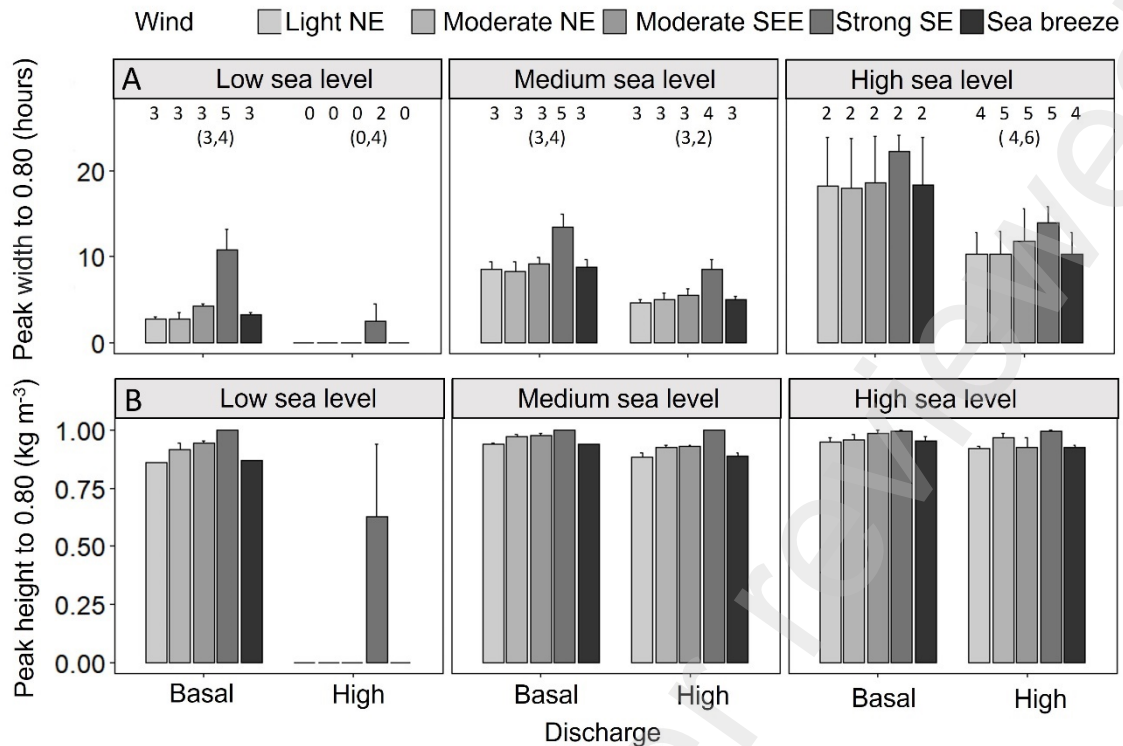
388

Sea level	Lag between water level peaks (min)	Spearman	Spearman (60 min lag)	Tracer peak width (h)	Tracer peak height ( $\text{kg m}^{-3}$ )
LSL	83	0.59 *	0.71 *	$2.7 \pm 0.4$	$0.86 \pm 0.00$
MSL	203	0.55 *	0.64 *	$8.4 \pm 1.6$	$0.94 \pm 0.00$
HSL	240	0.69 *	0.76 *	$18.2 \pm 9.8$	$0.95 \pm 0.02$

389

390

391 In the case of LSL and basal discharge, the number of intrusions remained at three  
 392 events for all wind conditions except the strong SE wind scenario, where five events  
 393 were recorded (Fig. 4 A). The duration and intensity were more significant in the strong  
 394 wind scenario (10.7 h and  $1.0 \text{ kg m}^{-3}$  of tracer concentration, respectively) compared to  
 395 the other wind conditions (2.6 to 4.2 h and  $0.86$  to  $0.94 \text{ kg m}^{-3}$ , respectively). The increase  
 396 in tributary discharge reduced the number of intrusions to two in the strong SE wind and  
 397 prevented them from occurring in the other wind scenarios. The increase in discharge  
 398 also caused a considerable decrease in the duration (to 2.5 h) and average intensity  
 399 (tracer concentration of  $0.63 \text{ kg m}^{-3}$ ) of the intrusion under strong wind conditions (Fig. 4  
 400 A and B).



401

402 Figure 4. A) Duration (peak width > 0.80 kg m<sup>-3</sup>) and B) Intensity (peak height > 0.80 kg  
 403 m<sup>-3</sup>) of marine intrusion in the channel (C1) in the different scenarios considered. The  
 404 numbers in the upper panels indicate the number of intrusions in the simulation days (72  
 405 h) and in parentheses the average.

406

407 Regarding the mean sea level (MSL) and basal river discharge scenarios, the number of  
 408 intrusions remained at three and reached five events under strong SE wind conditions.  
 409 The two tributary discharge scenarios showed a similar pattern in the intrusions (Fig. 4  
 410 A). The intrusion duration in the basal discharge scenario was longer in strong wind  
 411 conditions (13.4 h) than in other wind conditions (8.3 - 9.1 h). The intensity was also  
 412 more significant in the high wind conditions, but the differences with the other wind  
 413 scenarios were small, with all tracer concentrations > 0.94 kg m<sup>-3</sup>. In the high discharge  
 414 scenarios, the duration of intrusions decreased in all wind conditions (range: 4.6 - 8.4 h).  
 415 The intensity slightly reduced except in the strong wind scenario (with an average tracer  
 416 concentration of 1 kg m<sup>-3</sup>).

417

418 In the HSL and basal tributary discharge, two marine intrusions were recorded under all  
 419 wind conditions. Their mean duration was very long (range: 18.2 to 22.1 h), and the  
 420 intensity was more significant under strong wind conditions, with little variation compared  
 421 to the other wind conditions (all tracer concentrations > 0.96 kg m<sup>-3</sup>) (Fig. 4). In this case,  
 422 the high tributary discharge increased the number of intrusions in all wind conditions,

423 reaching the maximum values recorded, however, the duration of intrusions decreased  
424 in all cases (10.3 to 13.4 h). As with the MSL case, the intrusion intensity slightly  
425 decreased, except for the strong wind, which remained at  $1 \text{ kg m}^{-3}$ .

426

427 Overall, as the sea level increased, the occurrences of intrusions tended to decrease but  
428 lasted longer and were more intense. Interestingly, high tributary discharges appeared  
429 to increase the number of intrusions but to decrease their duration and intensity at MSL  
430 and HS, and prevent them at LSL. Winds had a lower effect than expected, where only  
431 strong SE winds tended to increase the duration and intensity of intrusions in all  
432 scenarios.

433

434

### 435 **4.3 Forcings relative importance in the duration and intensity of marine intrusions**

436

437 The CART results provide a complementary viewpoint to the previous analysis.  
438 According to CART, the forcing with higher relative importance in the duration of the  
439 intrusions was sea level (83%), followed much below by tributary discharge (16%) and  
440 wind (1%). The best regression model showed an average duration of the intrusions of  
441 19 h in the basal tributary discharge and 11 h in the high tributary discharge scenario  
442 under HSL conditions (Fig. 5 A). The duration of the intrusion was 7.7 h in MSL conditions  
443 and 2.5 h in LSL. The estimated prediction error for the model was 4.6 h. Wind was not  
444 considered as a forcing factor to differentiate between cases.

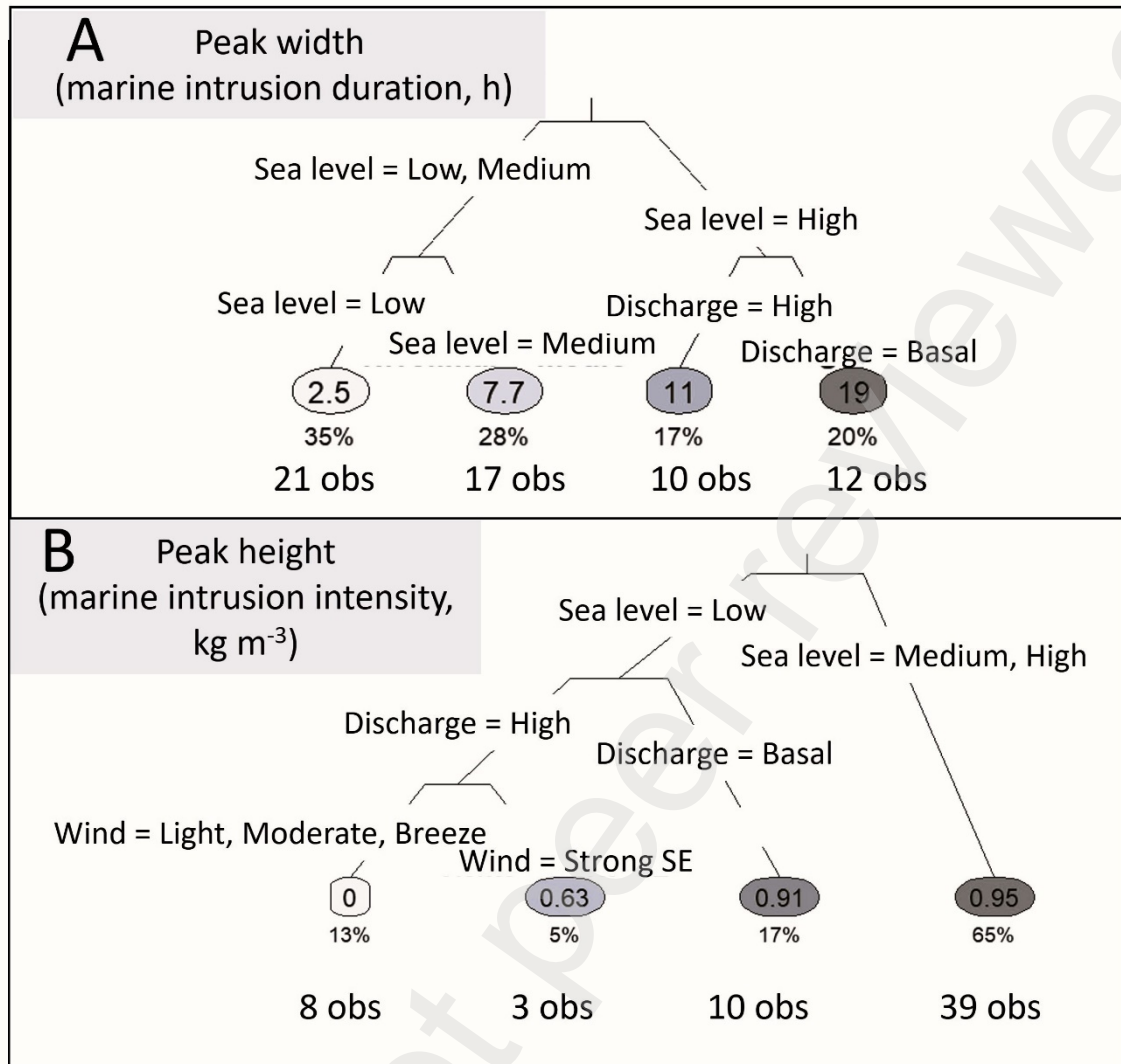
445

446 However, the intensity of the intrusions was mainly determined by the tributary discharge  
447 (46%), followed by sea level (40%) and much below wind (14%) as was shown by the  
448 CART model. The best regression model indicated an average intensity of the intrusions  
449 achieving  $0.95 \text{ kg m}^{-3}$  of tracer concentration under MSL or HSL conditions (Fig. 5 B).  
450 Values of tracer concentration of  $0.91 \text{ kg m}^{-3}$  were obtained in conditions of basal  
451 tributary discharge and  $0 \text{ kg m}^{-3}$  under LSL and high river discharge, showing a lower  
452 intensity of intrusions, except for strong SE winds that predicted an intensity average of  
453  $0.63 \text{ kg m}^{-3}$ . The prediction error for this model was  $0.034 \text{ kg m}^{-3}$ .

454

455

456



457

458 Figure 5. Regression tree diagram (CART) according to A) the duration and B) the  
 459 intensity of marine intrusions. Each diagram indicates the average duration or intensity  
 460 (light blue circles), the number of final observations of each terminal node and the  
 461 corresponding percentage.

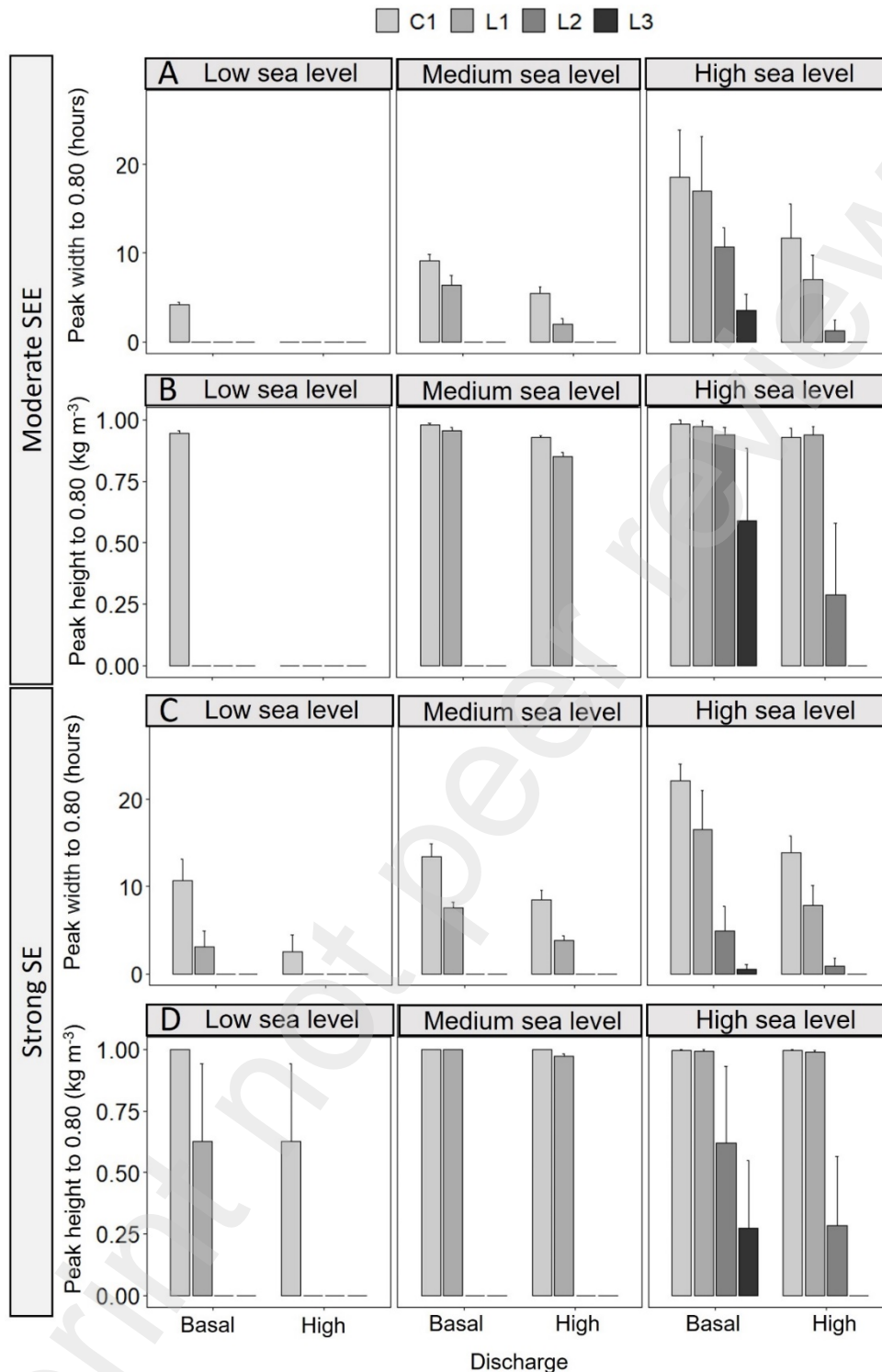
462

#### 463 4.4 Marine intrusions extent

464 The marine intrusions reached the furthest observation site (L3) under HSL and basal  
 465 tributary discharge (Fig. 6). Under LSL conditions, intrusions were only observed in the  
 466 channel, except under strong SE wind and basal tributary discharge conditions (Fig. 6).

467

468



469

470 Figure 6. Duration (width of peaks > 0.80 kg m<sup>-3</sup>) and intensity (height of peaks > 0.80  
 471 kg m<sup>-3</sup>) of marine intrusions in the different observation sites of the lagoon (C1, L1 to L3)  
 472 under moderate SEE wind (A and B panels) and strong SE wind (C and D panels)  
 473 conditions.

474 The duration of marine intrusions within the lagoon decreased as distance from the  
 475 channel increased for all sea level scenarios and both moderate SEE and strong SE

476 wind conditions (Fig. 6). Similarly, an increase in the duration of intrusions with increasing  
477 sea level was observed for both wind and tributary discharge conditions (Fig. 6).

478 The intensity of the intrusions was generally higher in C1 and L1, with tracer  
479 concentrations ranging from 0.62 to 1 kg m<sup>-3</sup>, and differed markedly from L2 and L3, with  
480 much lower concentrations (0.28 to 0.61 and 0.27 to 0.59 kg m<sup>-3</sup>, respectively) (Fig. 6).  
481 In L3, the duration and intensity of the marine intrusion was higher under conditions of  
482 moderate SEE wind, even exceeding that under strong SE wind (Fig. 6).

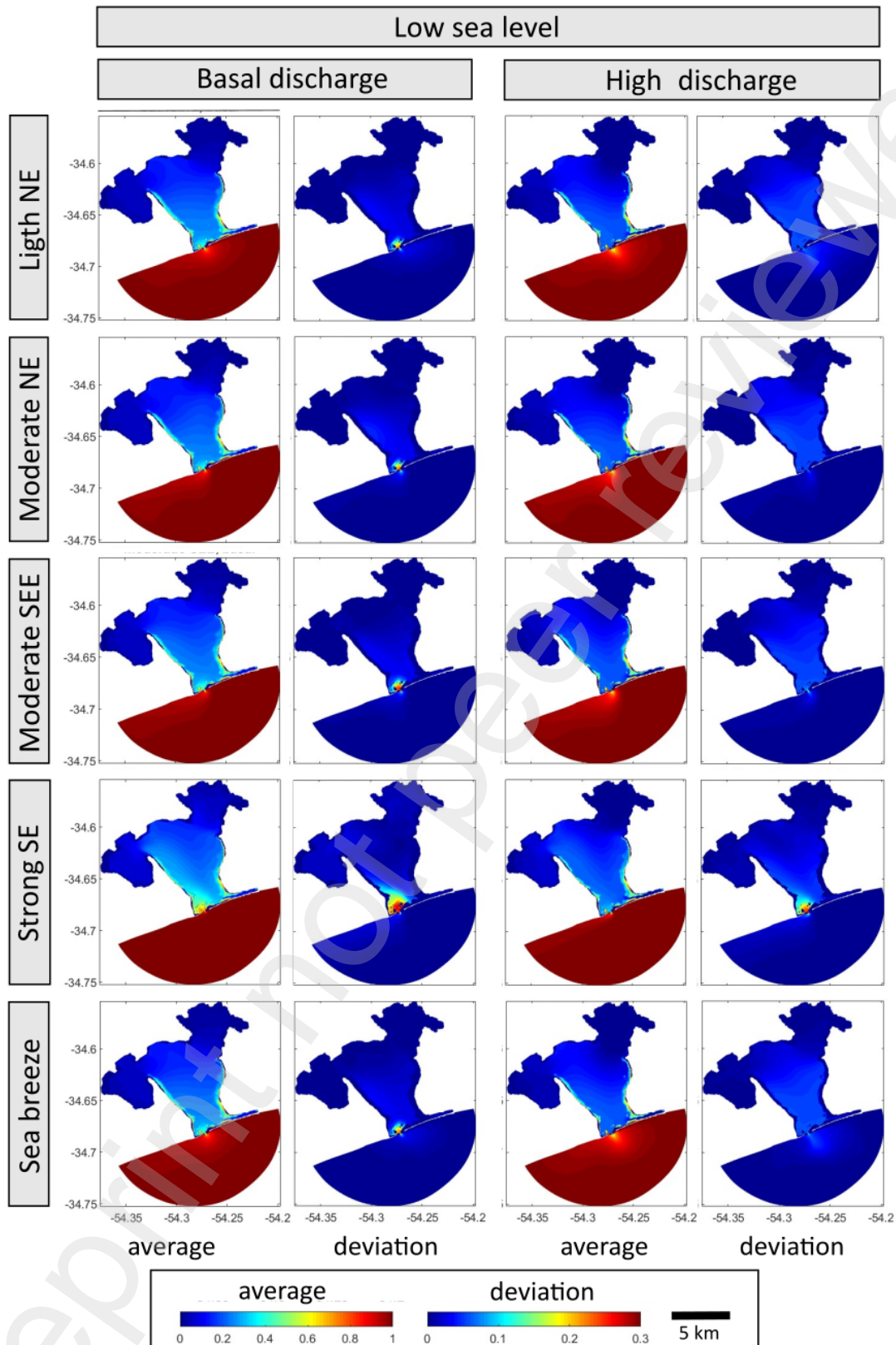
483 During LSL and basal tributary discharge, very low tracer concentrations (0.2 to 0.4 kg  
484 m<sup>-3</sup>) were observed over most of the lagoon surface. The highest concentrations were  
485 observed at the closed boundaries within the lagoon and the entrance channel zone.  
486 The standard deviation was higher in the vicinity of the channel and more significant  
487 during strong SE wind conditions (Fig. 7). The tracer concentration was even attenuated  
488 when the tributary discharge was high (< 0.2 kg m<sup>-3</sup>, Fig. 7).

489 Under MSL and basal tributary discharge, the influence of the tracer was observed in the  
490 middle zone of the lagoon (approx. 0.4 kg m<sup>-3</sup>). Nevertheless, it concentrated more in the  
491 channel zone (concentration > 0.6 kg m<sup>-3</sup>). The strong SE wind increased the average  
492 and deviation of the tracer concentration in the south-west part of the lagoon (Fig. 8). At  
493 high tributary discharge, the same spatial pattern as for basal tributary discharge was  
494 observed, but with a weakening of the tracer concentration throughout the study area. In  
495 this case, the standard deviation was higher in the channel zone compared to the  
496 standard deviation of the basal river discharge scenarios.

497 In the case of HSL and basal tributary discharge, the tracer concentration reached very  
498 high concentrations (approx. 0.8 – 1 kg m<sup>-3</sup>) and considerable deviations (. 0.4 – 0.6 kg  
499 m<sup>-3</sup>) in the central-southern part of the lagoon (Fig. 9). The moderate SEE and strong SE  
500 wind scenarios showed the highest concentrations of the tracer and also a “V” spatial  
501 distribution (higher concentrations at closed boundaries), which was more pronounced  
502 in the second scenario. This spatial distribution differs from the other wind scenarios  
503 where the concentration gradient was more homogeneous in the E-W direction or even  
504 showed an inverted “V” shape (lower concentrations at the edges) (Fig. 9). A similar  
505 pattern occurred for the tracer concentration in the high tributary discharge scenario,  
506 except that the concentrations were lower, and the deviations were higher (Fig. 9).

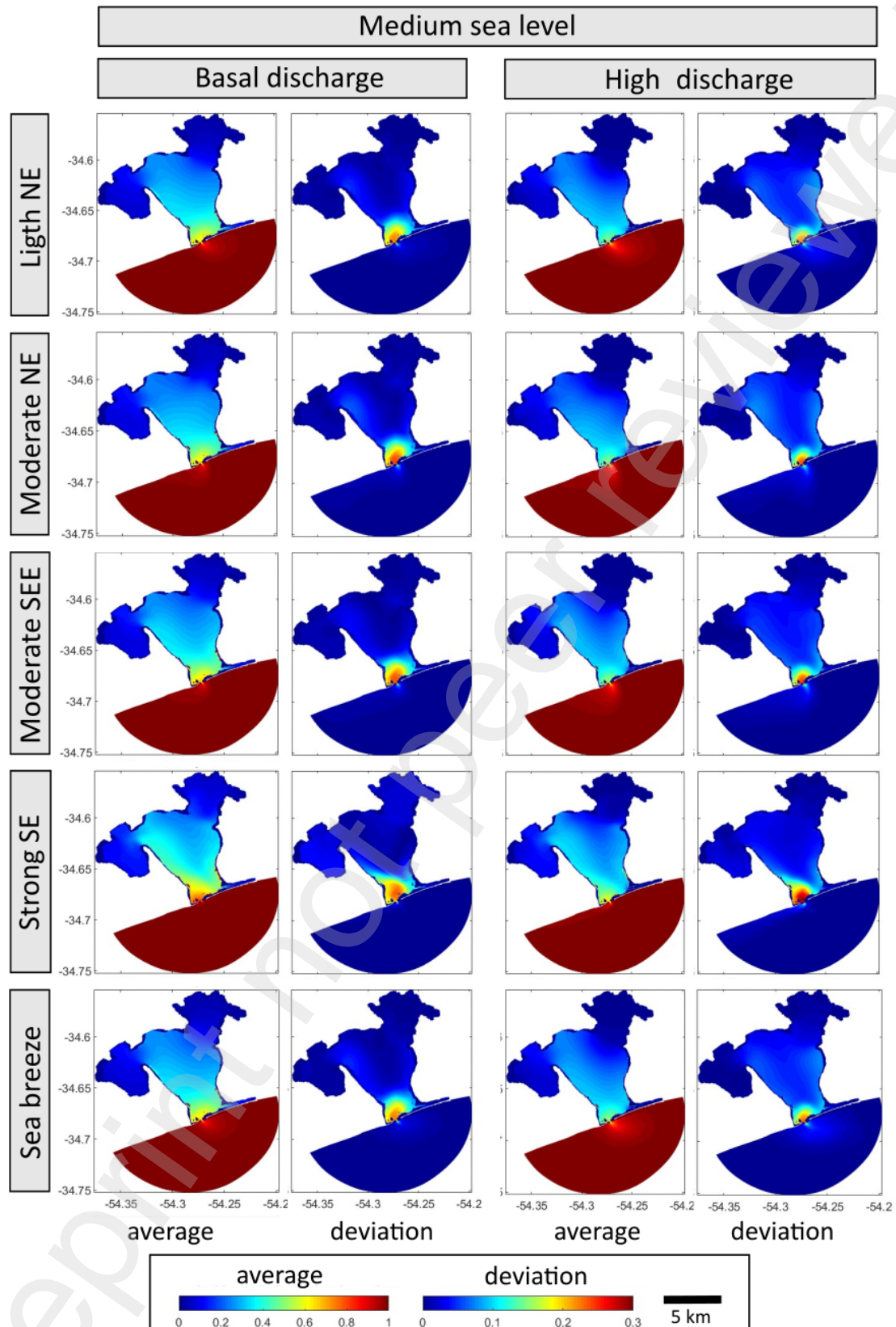
507

508



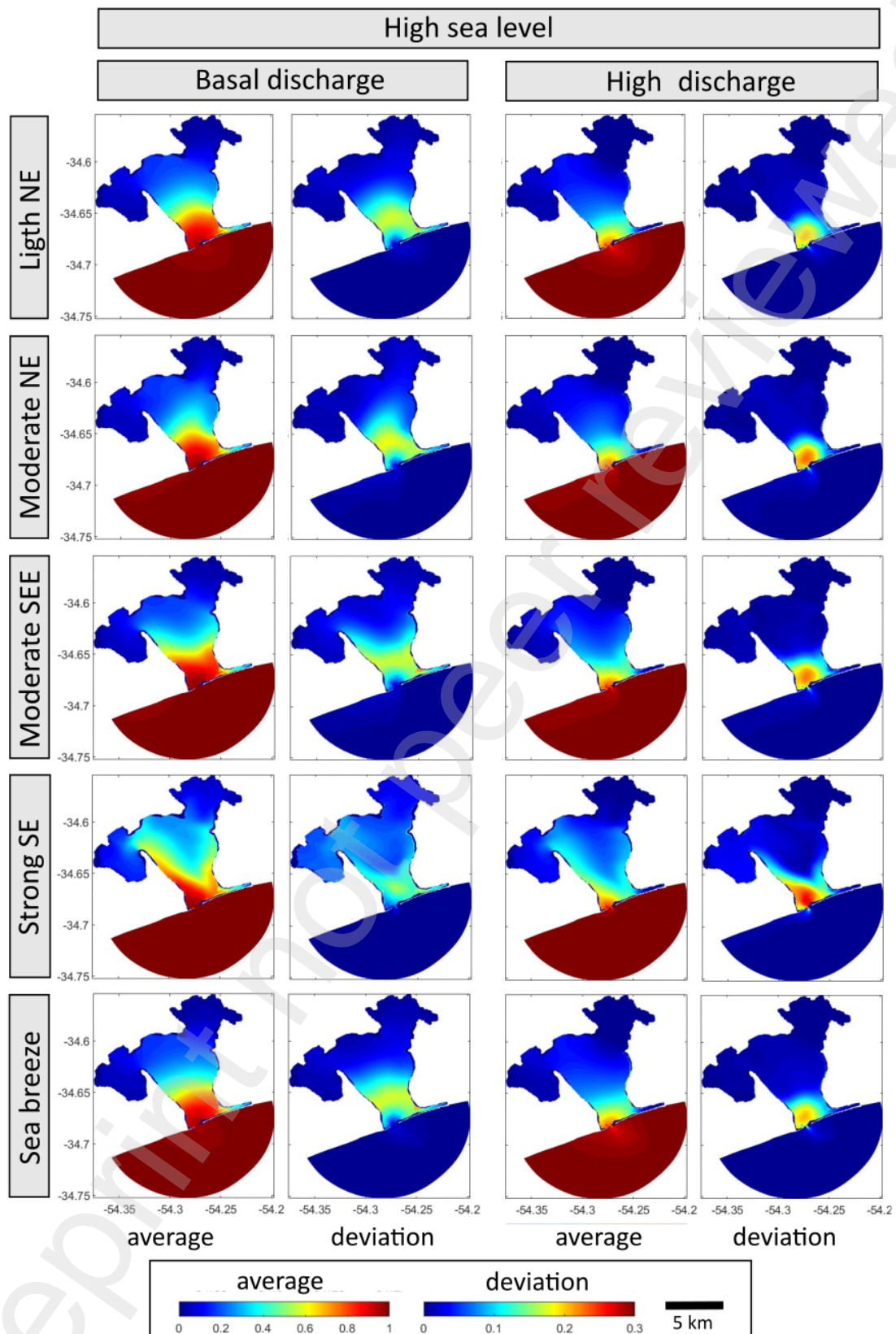
509

510 Figure 7. Average and standard deviation ( $\text{kg m}^{-3}$ ) of the tracer concentration for low-sea  
 511 level scenarios, under different wind (upper to lower panels) and discharge (left to right  
 512 panels) conditions.



513

514 Figure 8. Average and standard deviation ( $\text{kg m}^{-3}$ ) of the tracer concentration for medium-  
 515 sea level scenarios, under different wind (upper to lower panels) and discharge (left to  
 516 right panels) conditions.



517

518 Figure 9. Average and standard deviation ( $\text{Kg m}^{-3}$ ) of the tracer concentration for high-  
 519 sea level scenarios, under different wind (upper to lower panels) and discharge (left to  
 520 right panels) conditions.

## 521 **5 Discussion**

522 This study contributes to understanding the exchange process between a coastal lagoon  
523 and the adjacent sea and answers the questions established. The duration of marine  
524 intrusions was related to sea level; high sea levels and basal tributary discharge caused  
525 significantly longer intrusions (19 - 22 h). The intensity of the intrusions in the main  
526 channel was driven mainly by the tributary discharge and sea level. In conditions of low  
527 sea levels, short daily periods (2 - 4 h in duration) were favourable for the entry of  
528 seawater, mainly during the highest high tide, while marine intrusions were practically  
529 prevented or restricted to the channel zone when the sea level was low, and the tributary  
530 discharge was high. On the contrary, when the sea level was medium or high, the  
531 intrusions were observed in the central-southern area of the lagoon. The wind forcing  
532 had minor importance, reinforcing the intrusion processes in particular cases.

533

### 534 **5.1 Model validation**

535 The implemented model showed good performance in representing the water levels in  
536 LR. The RMSE values in this study were slightly above those reported in the modelling  
537 of the Laguna de los Patos (Martins et al. 2007) and the Ria de Aveiro (e.g. Vaz et al.  
538 2019), large systems with a permanent connection to the ocean through a channel of  
539 approx. 300 and 600 m wide, respectively. Therefore, a higher difference between  
540 observed and simulated values by the model in this study may be related to the  
541 simplifications assumed i.e. bathymetry and geomorphology remained unchanged  
542 during the simulation. Based on this simplification and the general precision of the model  
543 (RMSE, sub-optimal but in an acceptable range), it can be considered that the general  
544 characteristics of the circulation in the lagoon - particularly in the southern part - are  
545 satisfactorily captured by the model. Therefore, this constitutes a valuable tool for  
546 assessing marine intrusion processes in this lagoon.

547

### 548 **5.2 Marine intrusion dynamics**

549 This study showed that the duration and intensity of marine intrusions are very sensitive  
550 to sea level. The relationship between marine intrusions in the channel and the currents  
551 induced by the sea level has already been observed in a microtidal bay on the Texas  
552 coast (USA) (Brown et al. 2000). This study demonstrate that even under basal tributary  
553 discharge and each of the sea level scenarios, the maximum high tide exceeds a sea  
554 level that ensures at least one marine intrusion per day, despite being in a microtidal

555 regime. The CART analysis compared the impact of the three studied forcings and  
556 identified sea level as one of the most critical variables. However, this analysis also  
557 recognised the importance of tributary discharge and winds, the latter of lesser relative  
558 importance. This is crucial because these forcings, together with other variables,  
559 influence variations in sea levels (Teixeira 2019).

560 The main sea level variations on the Atlantic coast of Uruguay and the Río de la Plata  
561 respond to meteorological factors such as temperature, wind, and the Río de la Plata  
562 discharge, which combine differently depending on the spatio-temporal scale (D'Onofrio  
563 et al. 2008, Saraceno et al. 2014, Verocai et al. 2016). Regionally, higher sea levels in  
564 the study area are associated with strong SE (onshore) winds, storm surges originating  
565 from the Patagonian shelf, or a combination of both (Simionato et al. 2004, D'Onofrio et  
566 al. 2008, Verocai et al. 2016). On the contrary, lower sea levels along the Uruguayan  
567 coast occur under conditions of persistent northerly (offshore) winds (Verocai et al. 2016,  
568 Saraceno et al. 2014). Winds parallel to the coast also affect sea levels through Ekman  
569 transport. Winds from the SW, generally occurring in autumn-winter, tend to generate  
570 positive sea level anomalies on the Atlantic coast of Uruguay, while winds from the NE  
571 generate negative anomalies (Saraceno et al. 2014, Trinchín et al. 2019). Therefore, the  
572 sea level in the study area and regional wind dynamics are closely related, affecting the  
573 marine intrusions in LR. Nevertheless, local winds seem to be of minor importance,  
574 affecting the water exchange only at specific conditions.

575 According to the simulations, the most frequent winds in the study area (light NE,  
576 moderate NE, moderate SEE, sea breeze) did not directly generate marine intrusions,  
577 except for the strong SE wind. Despite being a less critical forcing, differences in the  
578 duration of the intrusion between winds of similar directions, such as moderate SEE and  
579 strong SE, indicate that wind intensity is a relevant parameter. On the other hand, studies  
580 in coastal lagoons have indicated that wind is the main factor in determining marine  
581 intrusions and larval ingress (Martins et al. 2007, Franzen et al. 2019). The main  
582 difference with our research was that those authors considered regional wind effects  
583 rather than local effects, such as local wind stress. To enhance our understanding of the  
584 impact of wind in marine intrusions into LR, it is of utmost importance to conduct further  
585 studies that consider a larger area for model implementation (e.g. nested models).

586 This study confirms that increasing the discharge from the lagoon during high tributary  
587 discharge conditions may prevent or limit the duration and intensity of marine intrusions  
588 with LSL. This is consistent with totally limnic conditions within a typical brackish lagoon  
589 (Laguna de los Patos, about 300 km north of LR) and evidence of large discharges into

590 the adjacent sea during a period of high rainfall (El Niño event) (Möller et al. 2009,  
591 Bitencourt et al 2020). The CART found significant effects of tributary discharge on the  
592 intensity of intrusions showing its higher impact with LSL. However, the duration of  
593 intrusions decreased under HSL, but the frequency of intrusions increased. Moreover, at  
594 the highest tributary discharge, a general pattern of larger tracer variability was observed  
595 in the southern area and the entrance channel, under all wind and sea level conditions.  
596 This suggests a greater exchange between the lagoon and the ocean in both directions  
597 occurs, as previously identified by Fiandrino et al. (2017). Therefore, it can be concluded  
598 that tributary discharge affects the dynamics of marine intrusion in microtidal coastal  
599 lagoons with limited connection to the ocean.

600 The prevailing conditions in the study area are light to moderate NE to SE winds (2-6 m  
601 s<sup>-1</sup>), a total tributary discharge < 18 m<sup>3</sup> s<sup>-1</sup> and an average sea level of 0.1 m with irregular  
602 semi-diurnal oscillations. However, studies based on historical data have observed  
603 changes in the trends of some meteorological variables (D'Onofrio et al. 2008, Verocai  
604 et al. 2016). For example, an increasing trend in annual precipitation has been observed  
605 since 1970 (Bidegain et al. 2012). Trends have also shown an increase in the frequency  
606 of heavy precipitation (> 25 mm day<sup>-1</sup>) and an increase in the frequency of droughts (e.g.  
607 Bidegain et al. 2012, Caorsi et al. 2018). Sea level rise (1 to 3 mm yr<sup>-1</sup>, for the period  
608 1955-2014), increased frequency of high sea level events and increasingly extreme sea  
609 level minima have also been observed (e.g. D'Onofrio et al. 2008, Verocai et al. 2016).  
610 These changes could affect the dynamics of marine intrusions in the coastal lagoons of  
611 Uruguay. For example, increased precipitation would tend to decrease the intensity and  
612 duration of marine intrusions. However, an increase in mean sea level would have the  
613 opposite effect, leading to a rise in the duration and intensity of intrusions. According to  
614 the results of this study, if these two opposing trends coincide, the result will be a higher  
615 frequency of intrusions and more significant variability of environmental conditions in the  
616 southern part of the lagoon and near the channel due to alternating marine intrusions  
617 and fluvial discharges (e.g. Fig. 4 A, 8 and 9). Nevertheless, different combinations of  
618 these climatic trends may raise the overall variability in the system, reducing predictability  
619 not only for managers but also for fishing resources and biodiversity as a whole.

620

### 621 **5.3 Conceptual model of LR hydrodynamics**

622 The current conceptual model of the hydrodynamics of LR (Conde et al. 2000, 2019)  
623 proposes an alternating cycle of lagoon phases, dependent on the state of the sanbar.  
624 This alternation may occur more than once a year and is summarised as limnetic and

625 uniform conditions in the closed sandbar phase versus a salinity gradient in the open  
626 sandbar phase (presence of an inlet), which in turn influences the lagoon biological  
627 communities (e.g Bonilla et al. 2005, Rodríguez-Gallego et al. 2015, Amaral et al. 2016,  
628 Machado et al. 2021). A conceptual model of the sandbar dynamic at shorter time scales  
629 has also been provided, describing the berm height and lagoon-ocean connectivity in  
630 relation to coastal (sediment accumulation, wave dynamics) and catchment (river  
631 discharge) processes (Conde et al. 2019). This study deepens the understanding of the  
632 short-term temporal and spatial variability resulting from the lagoon-ocean water  
633 exchange. The model highlights the high-frequency dynamic, with inflows and outflows  
634 of water occurring daily and sub-daily in the southern zone, in the vicinity of the channel.  
635 For example, seawater (with a salinity of greater than 70‰) or brackish water (with a  
636 salinity of less than 70‰) can be found in the vicinity of the channel, contingent on the  
637 time of day (Fig. 3). Variability increases during periods of high river discharge. Our  
638 results also demonstrated that sea level, tributary discharge and local winds are crucial  
639 in determining the frequency, duration, intensity and spatial extent of marine intrusions.  
640 In addition to the most evident south-north spatial gradient, lateral gradients in the lagoon  
641 (from west to east shore) have been previously proposed (Rodríguez-Graña et al. 2008,  
642 Espinosa et al. 2019) and were confirmed with our model.

643

#### 644 **5.4 Entry mechanism of estuarine-related meroplankton into microtidal coastal** 645 **lagoons**

646 The importance of sea level for the marine intrusion into LR shown in this study expands  
647 the possible conditions by which meroplankton may ingress into these microtidal systems  
648 (Whitfield et al. 2023). As has been shown, any arrangement of forcings that raise the  
649 sea level above the lagoon water level may allow the meroplankton to enter coastal  
650 lagoons. This explains why several studies conclude the importance of different factors  
651 in the influx of seawater and larvae into microtidal coastal lagoons, such as wind, tide,  
652 and sea breeze (Martins et al. 2007, Bruno and Acha 2015, Bruno et al. 2018). Moreover,  
653 even the main force that triggers the entry of seawater and larvae can vary over time in  
654 a single lagoon, as was shown in this study. Fish and decapod larvae without an  
655 endogenous cycle of vertical migration coupled to the tides detect incoming currents  
656 through changes in hydrostatic pressure, salinity, and temperature, among others  
657 (Rogers et al. 1993, Queiroga et al. 2006, Epifanio 2019). Larval behavioural responses  
658 include changes in swimming direction or swimming frequency and speed (kinesis) to  
659 accelerate the entry rate into the estuary (Epifanio 2019). Therefore, estuarine larvae on

660 the seaward side or in the lagoon access channel could detect incoming currents and  
661 initiate active behaviour to enter the lagoon.

662 Overall, we proposed that on the adjacent coast and in the inlet, larvae attempting to  
663 enter LR can select the incoming currents for larval transport, which, unlike the STST,  
664 may not be solely due to the flood tide effect. In turn, some studies have observed that  
665 larvae of an estuarine-related species known to use the STST mechanism also take  
666 advantage of wind-generated onshore current pulses (Joyeux 1998, Queiroga et al.  
667 2006). Even in environments where mesotidal amplitude and channel morphology (e.g.  
668 width, depth) are sufficient to generate tidal currents within estuaries, interannual  
669 variability in the maximum abundance of larval exporting portunid crabs has been linked  
670 to sporadic favourable wind-generated inflow events (e.g. Queiroga et al. 2006). The use  
671 of incoming currents by larvae, proposed for LR, may also be useful in other coastal  
672 lagoons, microtidal or mesotidal estuaries.

673 A possible mechanism for larval entrance in the microtidal LR is through the daily pulses  
674 generated by the highest tide every day, once larvae suitable for estuarine recruitment  
675 congregate in the adjacent marine zone. Meroplankton often show changes in activity  
676 associated with cyclical environmental factors such as day-night cycles and lunar phases  
677 (Wheeler and Epifanio 1978, Queiroga et al. 2006, Bruno et al. 2018). A common feature  
678 of most LR estuarine-related species or those phylogenetically related to them (e.g.  
679 megalopae of *C. sapidus* and *N. granulata*, decapodids of *Peaneus* spp. or peneids and  
680 larvae of *Micropogonias* spp. or croakers) is that larvae enter estuaries or bays during  
681 nighttime inflows (Olmi 1994, Cházaro-Olvera et al. 2009, Hale and Targett 2018).  
682 Additionally, the duration of these inflows impacts the abundance of the larvae, with  
683 higher numbers observed during longer inflows (e.g. Wenner et al. 2005, Biermann et al.  
684 2016). Based on the model simulations, this indicates that the greatest numbers of larvae  
685 will enter LR when sea levels are medium to high (e.g. marine intrusions > 8 h) as a  
686 result of interactions between various forces that lead to sea level increases (e.g.  
687 moderate to strong SE and SW winds, spring tides).

688 In addition, low recruitment has been reported in certain situations in coastal lagoons,  
689 indicating a barrier to larval entry. For example, prolonged periods of high freshwater  
690 discharge impede shrimp larval entry in a nearby coastal lagoon (Möller et al. 2009). This  
691 is consistent with the results of this study, where the duration and, ultimately, the  
692 frequency of marine intrusions decreased under conditions of high river discharge and  
693 low sea level. The current results align with the advection of most estuarine fish and  
694 decapod larvae towards the coastal zone observed in LR during a period of high rainfall

695 (Machado et al. 2021, Machado et al. unpublished). Similarly, some studies have shown  
696 that winds favoring lagoon discharge (Martins et al. 2007, Franzen et al. 2019) or  
697 withdrawing water from the coastal zone (e.g. upwelling), limit larval invasion (Queiroga  
698 et al. 2006).

699 The estuarine outflow, in turn, provides the chemical (humic substances, salinity) or  
700 physical (temperature, hydrostatic pressure) signals for larvae to locate the microtidal  
701 estuaries along the coast and congregate in front of them (Wheeler and Epifanio 1978,  
702 Epifanio 2019). This process is critical, as the number of larvae entering the estuary  
703 depends partly on the initial concentration of organisms outside (Miller and Shanks 2004,  
704 Queiroga et al. 2006, Santana et al. 2015). Once the estuarine-related fish larvae locate  
705 the estuary, the behaviour is usually triggered to remain in place until the conditions  
706 necessary to enter the estuary are met (e.g. Strydom 2003). Prolonged periods of no  
707 discharge from the lagoon to the coastal zone can prevent larval concentration in the  
708 nearshore, creating a bottleneck for recruitment within estuaries (Strydom 2003). The  
709 alternation of inflow and outflow observed in this study may ensure the entry of larvae  
710 and the emission of these signals. In turn, early juveniles of estuarine-related fish species  
711 have been reported to enter during the outflow phase by actively swimming behaviour  
712 (Whitfield et al 2023 and citations herein). Therefore, calm to moderate meteorological  
713 conditions that maintain a sea level and river discharge that allow an alternation of water  
714 flows in both directions could be the optimal conditions to facilitate the entry of more  
715 species at different stages of development.

716 In ICOLs such as several Uruguayan coastal lagoons, the presence of sandbars is one  
717 of the main factors impeding water and biological connectivity between lagoons and the  
718 ocean (Conde et al. 2000, 2019. Machado et al. 2021). In the case of the shrimp *P.*  
719 *paulensis*, the effect of the closed sandbar in preventing larval entry is very evident, with  
720 more frequent juvenile harvesting in lagoons with higher connectivity to the ocean  
721 (Fabiano and Santana 2006). Although the entry of estuarine-dependent larvae has been  
722 observed during overwash events, the exchange is usually lower than when the channel  
723 over the bar is opened (Tweddle and Froneman 2017, Machado et al 2021).

724

## 725 **6 Summary and conclusion**

726 The results of this study, which focused on the frequency, duration, intensity and extent  
727 of marine intrusions in the vicinity of LR channel, showed that conditions for larval influx  
728 occur daily during the analysed period and in the open inlet state. Sea level is highlighted  
729 as the main forcing determining the intrusions' duration. The higher the mean sea level,

730 the more extensive the marine intrusions are. Strong SE winds also tended to increase  
731 the duration of intrusions in all scenarios. Tributary discharge followed by sea level  
732 determined the intensity of marine intrusions; higher discharge attenuates, and higher  
733 sea level intensifies the marine intrusions. The intensity of intrusions was generally  
734 higher near the channel but can achieve central zones of the lagoon as the sea level  
735 increases.

736 In order to enhance the relevance of the regional scale for some of the factors evaluated  
737 (e.g. wind) may be necessary to implement the model with a larger marine area (e.g.  
738 nested models). Furthermore, water level measurements at different lagoon locations  
739 should be available to investigate further the effects of forcing on the spatial variation of  
740 marine intrusion within the lagoon.

741 Knowing the importance of sea level for marine intrusion in LR allows us to extend the  
742 number of recognised mechanisms by which meroplankton may enter these systems.  
743 For example, it could be any arrangement of forcings whose overlapping effect is to raise  
744 the sea level above the lagoon water level, achieving the different spatial extent of the  
745 marine intrusion according to that combination of forcings. The results suggest that even  
746 the main force that triggers the entry of seawater and therefore larvae can vary largely  
747 over time in a single lagoon. Therefore, we propose in LR a mechanism based on the  
748 selection of incoming currents for larval transport that, unlike the STST, may not be solely  
749 due to the flood tide effect.

750 Previous studies highlighted that one of the main determinants of larval entry for  
751 estuarine-related species is the duration of marine intrusions and the time of day they  
752 occur. Specifically, these studies found that larval entry is maximised when there is a  
753 high abundance of entry-competent larvae in the marine zone, sea level rises at night,  
754 and small or moderate tributary flows allow prolonged marine intrusions. In the study  
755 area, sea level rise is caused by a combination of astronomical and atmospheric factors.  
756 For example, in cases where spring tides, remote tides or winds (e.g. onshore or SW  
757 parallel winds) cause sea level rise, the signal is coincident and amplified.

758 These results are relevant for understanding and managing of LR protected area. On the  
759 one hand, knowledge of processes at small temporal and spatial scales will be improved  
760 by developing more precise study methods. Field studies to assess short-term changes  
761 in water conditions and the abundance of estuarine-related larvae near the entrance  
762 channel as a function of incoming currents are required to verify the proposed  
763 mechanism. On the other hand, the protocol for the artificial opening of the sandbar is  
764 based only on conditions that influence the lagoon water level with watershed origin (e.g.,

765 rainfall forecast) (Conde et al. 2019). The results of this study showed the importance of  
766 other factors in the lagoon-ocean exchange, such as sea level, which should be included  
767 as criteria to complement future management decisions, if fisheries - other than water  
768 quality - are also intended to be preserved.

769

Preprint not peer reviewed

770 **Acknowledgements**

771 The authors thank the Instituto Nacional de Meteorología of Uruguay (INUMET) for the  
772 distribution of air temperature and rainfall data, the Servicio de Oceanografía, Hidrografía  
773 y Meteorología de la Armada of Uruguay (SOHMA) for the distribution of *in situ* sea level  
774 data, the Copernicus Marine Service website for the distribution of sea level data, and  
775 the Universidad de la República (Uruguay) for the bathymetry, tributary discharge and  
776 wind data. Special thanks to C. Chreties, G. Manta,, S. Solari and M. Teixeira. I. Machado  
777 extends her gratitude to all colleagues of the Nucleo de Modelação Hidrodinâmica da  
778 Universidade de Aveiro (Portugal). This study was possible due to the funds provided in  
779 Uruguay by PEDECIBA Doctoral Program, CSIC (UdelaR) doctoral fellowship, CSIC  
780 (UdelaR) Programa de Movilidad e Intercambios Académicos and ANII  
781 (FCE\_1\_2017\_1\_136178). The authors acknowledge financial support to CESAM by  
782 FCT/MCTES (UIDP/50017/2020 + UIDB/50017/2020 + LA/P/0094/2020) through  
783 national funds.

784

785 **References**

- 786 Alonso, R., Jackson, M., Santoro, P., Fossati, M., Solari, S., Teixeira, L., 2017. Wave  
787 and tidal energy resource assessment in Uruguayan shelf seas. *Renewable*  
788 *Energy*. 114, 18–31. <https://doi.org/10.1016/j.renene.2017.03.074>
- 789 Amaral, V., Graeber, D., Calliari, D., Alonso, C., 2016. Strong linkages between DOM  
790 optical properties and main clades of aquatic bacteria. *Limnology and*  
791 *Oceanography*. 61(3), 906–918. <https://doi.org/10.1002/lno.10258>
- 792 Amaral, V., Romera-Castillo, C., García-Delgado, M., Gómez-Parra, A., Forja, J., 2020.  
793 Distribution of dissolved organic matter in estuaries of the southern Iberian  
794 Atlantic Basin: Sources behavior and export to the coastal zone. *Marine*  
795 *Chemistry*. 226, 103857. <https://doi.org/10.1016/j.marchem.2020.103857>
- 796 Barreiro, M., Arizmendi, F., Trinchin, R., 2019. Variabilidad y Cambio Climático en  
797 Uruguay. In: Plan Nacional de Adaptación Costera y el Plan Nacional de  
798 Adaptación en Ciudades, Convenio MVOTMA-UdelaR Proyecto PNUD-  
799 URU/16/G34
- 800 Bas, C., Luppi, T., Spivak, E., Schejter, L., 2009. Larval dispersion of the estuarine crab  
801 *Neohelice granulata* in coastal marine waters of the Southwest Atlantic.  
802 *Estuarine, Coastal and Shelf Science*. 83(4), 569–576.  
803 <https://doi.org/10.1016/j.ecss.2009.05.004>
- 804 Bidegain, M., Crisci, C., del Puerto, L., Inda, H., Mazzeo, N., Taks, J., Terra, R., 2012.  
805 Clima de cambios. Nuevos desafíos de adaptación en Uruguay. *Variabilidad*  
806 *climática de importancia para el sector productivo*. (FAO-MGAP. Vol. 1), 125 pp.
- 807 Biermann, J.L., North, E.W., Boicourt, W.C., 2016. The Distribution of blue crab  
808 (*Callinectes sapidus*) megalopae at the mouths of Chesapeake and Delaware  
809 Bays: Implications for larval ingress. *Estuaries and Coasts*. 39(1), 201–217.  
810 <https://doi.org/10.1007/s12237-015-9978-7>
- 811 Bitencourt, L.P., Fernandes, E.H.L, Moller, O., Ross, L., 2020. The contribution of ENSO  
812 cycles to the salinity spatio-temporal variability in a bar-built microtidal estuary.  
813 *Regional Studies in Marine Science*. <https://doi.org/10.1016/j.rsma.2020.101496>
- 814 Bonilla, S., Conde, D., Aubriot, L., Pérez, M.C., (2005). Influence of hydrology on  
815 phytoplankton species composition and life strategies in a subtropical coastal  
816 lagoon periodically connected with the Atlantic Ocean. *Estuaries*. 28(6), 884–895.  
817 <https://doi.org/10.1007/BF02696017>
- 818 Brown, C.A., Jackson, G.A., Brooks, D.A., 2000. Particle transport through a narrow tidal  
819 inlet due to tidal forcing and implications for larval transport. *Journal of*  
820 *Geophysical Research: Oceans*. 105(C10), 24141–24156.  
821 <https://doi.org/10.1029/2000JC000211>
- 822 Bruno, D.O., Acha, E., 2015. Winds vs. Tides: Factors ruling the recruitment of larval and  
823 juvenile fishes into a micro-tidal and shallow choked lagoon (Argentina).  
824 *Environmental Biology of Fish*. 98(5), 1449–1458.

- 825 Bruno, D.O., Delpiani, S.M., Acha, E.M., 2018. Diel variation of ichthyoplankton  
826 recruitment in a wind-dominated temperate coastal lagoon (Argentina).  
827 Estuarine, Coastal and Shelf Science. 205, 91–99.  
828 <https://doi.org/10.1016/j.ecss.2018.03.015>
- 829 Caorsi, M.L., Cruz, G., Terra, R., Astigarraga, L., Caorsi, M.L., Cruz, G., Terra, R.,  
830 Astigarraga, L., 2018. Variación de la precipitación y la ocurrencia de sequías en  
831 la cuenca lechera del SW del Uruguay en el período 1939—2011. *Agrociencia*  
832 (Uruguay). 22(1), 116–123. <https://doi.org/10.31285/agro.22.1.12>
- 833 Carballo, R., Iglesias, G., Castro, A., 2009. Residual circulation in the Ría de Muros (NW  
834 Spain): A 3D numerical model study. *Journal of Marine Systems*. 75(1), 116–130.  
835 <https://doi.org/10.1016/j.jmarsys.2008.08.004>
- 836 Cházaro-Olvera, S., Winfield, I., Coria-Olvera, V., 2009. Transport of *Farfantepenaeus*  
837 *aztecus* postlarvae in Three Lagoon-System Inlets in the Southwestern Gulf of  
838 Mexico. *Crustaceana*. 82(4), 425–437. <http://www.jstor.org/stable/27743297>
- 839 Conde, D., Aubriot, L., Sommaruga, R., 2000. Changes in UV penetration associated  
840 with marine intrusions and freshwater discharge in a shallow coastal lagoon of  
841 the Southern Atlantic Ocean. *Marine Ecology Progress Series*. 207, 19–31.  
842 <https://doi.org/10.3354/meps207019>
- 843 Conde, D., Solari, S., de Álava, D., Rodríguez-Gallego, L., Verrastro, N., Chreties, C.,  
844 Lagos, X., Piñeiro, G., Teixeira, L., Seijo, L., Vitancurt, J., Caymaris, H., Panario,  
845 D., 2019. Ecological and social basis for the development of a sand barrier  
846 breaching model in Laguna de Rocha. *Uruguay. Estuarine, Coastal and Shelf*  
847 *Science*. 219, 300–316. <https://doi.org/10.1016/j.ecss.2019.02.003>
- 848 De'ath, G., Fabricius, K., 2000. Classification and regression trees: A powerful yet simple  
849 technique for ecological data analysis *Ecology*. Wiley Online Library.  
850 [https://esajournals.onlinelibrary.wiley.com/doi/abs/10.1890/0012-9658\(2000\)](https://esajournals.onlinelibrary.wiley.com/doi/abs/10.1890/0012-9658(2000))
- 851 Días, J.M., Pereira, F., Picado, A., Lopes, C.L., Pinheiro, J.P., Lopes, S.M., Pinho, P.G.,  
852 2021. A comprehensive estuarine hydrodynamics-salinity study: impact of  
853 morphologic changes on Ria de Aveiro (Atlantic Coast of Portugal). *Journal of*  
854 *Marine Science and Engineering*. 9(2), 234. <https://doi.org/10.3390/jmse9020234>
- 855 Dias, J.M., Sousa, M.C., Bertin, X., Fortunato, A.B., Oliveira, A., 2009. Numerical  
856 modeling of the impact of the Ancão Inlet relocation (Ria Formosa, Portugal).  
857 *Environmental Modelling & Software*. 24(6), 711–725.  
858 <https://doi.org/10.1016/j.envsoft.2008.10.017>
- 859 Dickey-Collas, M., Bolle, L.J., Beek, J.K.L., van Erftemeijer, P.L.A., 2009. Variability in  
860 transport of fish eggs and larvae. II. Effects of hydrodynamics on the transport of  
861 Downs herring larvae. *Marine Ecology Progress Series*. 390, 183–194.  
862 <https://doi.org/10.3354/meps08172>
- 863 D'Onofrio, E.E., Fiore, M.M.E., Pousa, J.L. 2008. Changes in the regime of storm surges  
864 at Buenos Aires, Argentina. *Journal of Coastal Research*. 24(sp1), 260–265.  
865 <https://doi.org/10.2112/05-0588.1>

- 866 D'Onofrio, E.E., Fiore, M.M.E., Romero, S.I., 1999. Return periods of extreme water  
867 levels estimated for some vulnerable areas of Buenos Aires. *Continental Shelf*  
868 *Research*. 19(13). 1681–1693. [https://doi.org/10.1016/S0278-4343\(98\)00115-0](https://doi.org/10.1016/S0278-4343(98)00115-0)
- 869 Epifanio, C.E., 2019. Early Life History of the Blue Crab *Callinectes sapidus*: A Review.  
870 *Journal of Shellfish Research*. 38(1). 1–22. <https://doi.org/10.2983/035.038.0101>
- 871 Epifanio, C.E., Valenti, C.C., Pembroke, A.E., 1984. Dispersal and recruitment of blue  
872 crab larvae in Delaware Bay. *U.S.A. Estuarine, Coastal and Shelf Science*. 18(1),  
873 1–12. [https://doi.org/10.1016/0272-7714\(84\)90002-7](https://doi.org/10.1016/0272-7714(84)90002-7)
- 874 Espinosa, N., Calliari, D., Rodríguez-Graña, L., 2019. Life history, population structure  
875 and environmental modulation of *Neomysis americana* (Mysinae) in an  
876 intermittently open coastal lagoon of the South West Atlantic. *Estuarine, Coastal*  
877 *and Shelf Science*. 223, 129–137. <https://doi.org/10.1016/j.ecss.2019.04.019>
- 878 Fabiano, G., Santana, O., 2006. Las pesquerías en las lagunas costeras salobres de  
879 Uruguay. In: *Bases para la conservación y el manejo de la costa uruguaya*. Vida  
880 Silvestre, Montevideo. 557–565 pp.
- 881 Fernandes, E.H.L., Dyer, K.R., Moller, O.O., Niencheski, L.F.H., 2002. The Patos  
882 Lagoon hydrodynamics during an El Niño event (1998). *Continental Shelf*  
883 *Research*. 22(11), 1699–1713. [https://doi.org/10.1016/S0278-4343\(02\)00033-X](https://doi.org/10.1016/S0278-4343(02)00033-X)
- 884 Fiandrino, A., Ouisse, V., Dumas, F., Lagarde, F., Pete, R., Malet, N., Le Noc, S., de Wit,  
885 R., 2017. Spatial patterns in coastal lagoons related to the hydrodynamics of  
886 seawater intrusion. *Marine Pollution Bulletin*. 119(1), 132–144.  
887 <https://doi.org/10.1016/j.marpolbul.2017.03.006>
- 888 Franzen, M.O., Muelbert, J.H., Fernandes, E.H., 2019. Influence of wind events on the  
889 transport of early stages of *Micropogonias furnieri* (Desmarest. 1823) to a  
890 subtropical estuary. *Latin American Journal of Aquatic Research*. 47(3), 536–  
891 546. <https://doi.org/10.3856/vol47-issue3-fulltext-15>
- 892 Hale, E.A., Targett, T.E., 2018. Vertical distribution of larval Atlantic menhaden  
893 (*Brevoortia tyrannus*) and Atlantic croaker (*Micropogonias undulatus*):  
894 Implications for vertical migratory behaviour and transport. *Fisheries*  
895 *Oceanography*. 27(3), 222–231. <https://doi.org/10.1111/fog.12247>
- 896 Hothorn, T., Zeileis, A., 2015. partykit: A modular toolkit for recursive partytioning in R.  
897 *Journal of Machine Learning Research*. 16(118), 3905–3909.
- 898 Iles, T.D., Sinclair, M., 1982. Atlantic herring: stock discreteness and abundance.  
899 *Science*. 215(4533), 627–633. <https://doi.org/10.1126/science.215.4533.627>
- 900 Instituto Uruguayo de Meteorología (s.f.). Estadísticas climatólogicas: Características  
901 climáticas. [https://www.inumet.gub.uy/clima/estadisticas-](https://www.inumet.gub.uy/clima/estadisticas-climatologicas/caracteristicas-climaticas)  
902 [climatologicas/caracteristicas-climaticas](https://www.inumet.gub.uy/clima/estadisticas-climatologicas/caracteristicas-climaticas). Accessed 20.11.2021
- 903 Jager, Z., 1999. Selective tidal stream transport of flounder larvae (*Platichthys flesus*) in  
904 the Dollard (Ems Estuary). *Estuarine, Coastal and Shelf Science*. 49(3), 347–  
905 362. <https://doi.org/10.1006/ecss.1999.0504>

- 906 Joyeux, J.C., 1998. Spatial and temporal entry patterns of fish larvae into North Carolina  
907 Estuaries: Comparisons among one pelagic and two demersal species.  
908 Estuarine, Coastal and Shelf Science. 47(6), 731–752.  
909 <https://doi.org/10.1006/ecss.1998.0378>
- 910 Lesser, G.R., Roelvink, J.A., van Kester, J.A., Stelling, G.S., 2004. Development and  
911 validation of a three-dimensional morphological model. Coastal Engineering.  
912 51(8), 883–915. <https://doi.org/10.1016/j.coastaleng.2004.07.014>
- 913 Machado, I., Rodríguez-Gallego, L., Lescano, C., Calliari, D., 2021. Species-specific  
914 traits and the environment drive ichthyoplankton fluxes between an intermittently  
915 closed-open lagoon and adjacent coastal waters. Estuarine, Coastal and Shelf  
916 Science. 261, 107549. <https://doi.org/10.1016/j.ecss.2021.107549>
- 917 Manta, G., 2017. Caracterización de la brisa marina en Uruguay. Master Thesis.  
918 Universidad de la República. <https://hdl.handle.net/20.500.12008/21451>
- 919 Manta, G., Barreiro, M., Renom, M., 2021. Climatología de la brisa marina en Uruguay.  
920 Meteorologica. 46(1), 1–14. <https://doi.org/10.24215/1850468Xe002>
- 921 Martins, I.M., Dias, J.M., Fernandes, E.H., Muelbert, J.H., 2007. Numerical modelling of  
922 fish eggs dispersion at the Patos Lagoon estuary—Brazil. Journal of Marine  
923 Systems. 68(3), 537–555. <https://doi.org/10.1016/j.jmarsys.2007.02.004>
- 924 McSweeney, S.L., Kennedy, D.M., Rutherford, I.D., Stout, J.C., 2017. Intermittently  
925 Closed/Open Lakes and Lagoons: Their global distribution and boundary  
926 conditions. Geomorphology. 292, 142–152.  
927 <https://doi.org/10.1016/j.geomorph.2017.04.022>
- 928 de Mello, C., Barreiro, M., Ortega, L., Trinchín, R., Manta, G., 2022. Coastal upwelling  
929 along the Uruguayan coast: Structure, variability and drivers. Journal of Marine  
930 Systems. 230, 103735. <https://doi.org/10.1016/j.jmarsys.2022.103735>
- 931 Miller J., Shanks, A., 2004. Ocean-estuary coupling in the Oregon upwelling region:  
932 Abundance and transport of juvenile fish and of crab megalopae. Marine Ecology  
933 Progress Series. 271. 267–279. doi:10.3354/meps271267
- 934 Möller, O.O., Castello, J.P., Vaz, A.C. 2009. The effect of river discharge and winds on  
935 the interannual variability of the pink shrimp *Farfantepenaeus paulensis*  
936 production in Patos Lagoon. Estuaries and Coasts. 32(4), 787–796.  
937 <https://doi.org/10.1007/s12237-009-9168-6>
- 938 Narbondo, S., Gorgoglione, A., Crisci, M., Chreties, C., 2020. Enhancing physical  
939 similarity approach to predict runoff in Ungauged Watersheds in Sub-Tropical  
940 Regions. Water. 12(2), 528. <https://doi.org/10.3390/w12020528>
- 941 Ogburn, M.B., Criales, M.M., Thompson, R.T., Browder, J.A., 2013. Endogenous  
942 swimming activity rhythms of postlarvae and juveniles of the penaeid shrimp  
943 *Farfantepenaeus aztecus*, *Farfantepenaeus duorarum*, and *Litopenaeus*  
944 *setiferus*. Journal of Experimental Marine Biology and Ecology. 440, 149–155.  
945 <https://doi.org/10.1016/j.jembe.2012.12.007>

- 946 Olmi, E., 1994. Vertical migration of blue crab *Callinectes sapidus* megalopae:  
947 Implications for transport in estuaries. Marine Ecology Progress Series. 113, 39–  
948 54. <https://doi.org/10.3354/meps113039>
- 949 Perrin, C., Michel, C., Andréassian, V., 2003. Improvement of a parsimonious model for  
950 streamflow simulation. Journal of Hydrology. 279(1), 275–289.  
951 [https://doi.org/10.1016/S0022-1694\(03\)00225-7](https://doi.org/10.1016/S0022-1694(03)00225-7)
- 952 Pineda, J., Hare, J.A., Sponaugle, S., 2007. Larval transport and dispersal in the coastal  
953 ocean and consequences for population connectivity. Oceanography. 20(3), 22–  
954 39. <https://doi.org/10.5670/oceanog.2007.27>
- 955 Piola, A., Romero, S., Zajaczkovski, U., 2008. Space– time variability of the Plata plume  
956 inferred from ocean color. Continental Shelf Research, 28, 1556–1567.  
957 <https://doi.org/10.1016/j.csr.2007.02.013>
- 958 Queiroga, H., Almeida, M.J., Alpuim, T., Flores, A.A.V., Francisco, S., González-Gordillo,  
959 I., Miranda, A.I., Silva, I., Paula, J., 2006. Tide and wind control of megalopal  
960 supply to estuarine crab populations on the Portuguese west coast. Marine  
961 Ecology Progress Series. 307, 21–36. <https://doi.org/10.3354/meps307021>
- 962 Queiroga, H., Blanton, J., 2005. Interactions between behaviour and physical forcing in  
963 the control of horizontal transport of decapod crustacean larvae. Advances in  
964 Marine Biology. 47, 107–214. [https://doi.org/10.1016/S0065-2881\(04\)47002-3](https://doi.org/10.1016/S0065-2881(04)47002-3)
- 965 Rodó, E., 2013. Dinámica de los ciclos biogeoquímicos de nitrógeno y fósforo en la  
966 Laguna de Rocha. Master Thesis. Universidad de la República. 86 pp.  
967 <https://hdl.handle.net/20.500.12008/9071>
- 968 Rodríguez-Gallego, L., Achkar, M., Defeo, O., Vidal, L., Meerhoff, E., Conde D., 2017.  
969 Effects of land use changes on eutrophication indicators in five coastal lagoons  
970 of the Southwestern Atlantic Ocean. Estuarine, Coastal and Shelf Science. 188,  
971 116–126. <https://doi.org/10.1016/j.ecss.2017.02.010>
- 972 Rodríguez-Gallego, L., Sabaj, V., Masciadri, S., Kruk, C. Arocena, R., Conde, D., 2015.  
973 Salinity as a major driver for submerged aquatic vegetation in coastal lagoons: a  
974 multi-year analysis in the subtropical Laguna de Rocha. Estuaries and Coasts.  
975 38(2), 451–465. <https://doi.org/10.1007/s12237-014-9842-1>
- 976 Rodríguez-Graña, L., Calliari, D., Conde, D., Sellanes, J., Urrutia, R., 2008. Food web of  
977 a SW Atlantic shallow coastal lagoon: spatial environmental variability does not  
978 impose substantial changes in the trophic structure.  
979 <https://doi.org/10.3354/meps07401>
- 980 Rogers, B.D., Shaw, R.F., Herke, W.H., Blanchet, R.H., 1993. Recruitment of postlarval  
981 and juvenile brown shrimp (*Penaeus aztecus* Ives) from offshore to estuarine  
982 waters of the Northwestern Gulf of Mexico. Estuarine, Coastal and Shelf Science.  
983 36(4), 377–394. <https://doi.org/10.1006/ecss.1993.1023>
- 984 Roy, P.S., Williams, R.J., Jones, A.R., Yassini, I., Gibbs, P.J., Coates, B., West R.J.,  
985 Scanes, P.R., Hudson, J.P., Nichol, S., 2001. Structure and function of south-  
986 east Australian estuaries. Estuarine, Coastal and Shelf Science, 53(3), 351–384.  
987 <https://doi.org/10.1006/ecss.2001.0796>

- 988 Santana, O., Silveira, S., Fabiano, G., 2015. Catch variability and growth of pink shrimp  
 989 (*Farfantepenaeus paulensis*) in two coastal lagoons of Uruguay and their  
 990 relationship with ENSO events. Brazilian Journal of Oceanography. 63 (3).  
 991 [https://www.scielo.br/scielo.php?script=sci\\_arttext&pid=S1679-](https://www.scielo.br/scielo.php?script=sci_arttext&pid=S1679-87592015000300355&lng=en&tlng=en)  
 992 [87592015000300355&lng=en&tlng=en](https://www.scielo.br/scielo.php?script=sci_arttext&pid=S1679-87592015000300355&lng=en&tlng=en)
- 993 Saraceno, M., Simionato, C.G., Ruiz-Etcheverry, L.A., 2014. Sea surface height trend  
 994 and variability at seasonal and interannual time scales in the Southeastern South  
 995 American continental shelf between 27°S and 40°S. Continental Shelf Research.  
 996 91, 82–94. <https://doi.org/10.1016/j.csr.2014.09.002>
- 997 Simionato, C.G., Berasategui, A., Meccia, V.L., Acha M., Mianzan, H., 2008. On the short  
 998 time-scale wind forced variability in the Rio de la Plata estuary and its role on  
 999 ichthyoplankton retention. Estuarine, Coastal and Shelf Science. 76, 211–226.
- 1000 Simionato, C.G., Dragani, W., Nuñez, M., Engel, M., 2004. A set of 3-D nested models  
 1001 for tidal propagation from the Argentinean continental shelf to the Río de la Plata  
 1002 estuary—Part I. M2. Journal of Coastal Research. 20(3), 893–912.
- 1003 Sousa, M.C., Ribeiro, A.S., Des, M., Mendes, R., Alvarez, I., Gomez-Gesteira, M., Dias,  
 1004 J.M., 2018. Integrated High-resolution Numerical Model for the NW Iberian  
 1005 Peninsula Coast and Main Estuarine Systems. Journal of Coastal Research.  
 1006 85(sp1), 66–70. <https://doi.org/10.2112/SI85-014.1>
- 1007 Strydom, N.A., 2003. Occurrence of larval and early juvenile fishes in the surf zone  
 1008 adjacent to two intermittently open estuaries, South Africa. Environmental Biology  
 1009 of Fishes. 66(4), 349–359. <https://doi.org/10.1023/A:1023949607821>
- 1010 Tankersley, R.A., 2001. Selective Tidal-Stream transport of marine animals. In  
 1011 Oceanography and Marine Biology. An Annual Review. (Vol. 39). CRC Press.
- 1012 Teixeira, M., 2019. Modelos morfodinámicos aplicados a la gestión de las lagunas  
 1013 litorales. Master Thesis. Universidad de la República. 134 pp.  
 1014 <https://hdl.handle.net/20.500.12008/20935>
- 1015 Therneau, T. M., Atkinson, E.J., Foundation, M., 2022. An Introduction to Recursive  
 1016 Partitioning Using the RPART Routines. [https://cran.r-](https://cran.r-project.org/web/packages/rpart/)  
 1017 [project.org/web/packages/rpart/](https://cran.r-project.org/web/packages/rpart/)
- 1018 Trinchin, R., Ortega, L., Barreiro, M., 2019. Spatiotemporal characterization of summer  
 1019 coastal upwelling events in Uruguay, South America. Regional Studies in Marine  
 1020 Science. 31. 100787. <https://doi.org/10.1016/j.rsma.2019.100787>
- 1021 Tuchkovenko, Y., Tuchkovenko, O., Khokhlov, V., 2019. Modelling water exchange  
 1022 between coastal elongated lagoon and sea: Influence of morphometric  
 1023 characteristics of connecting channel on water renewal in lagoon. EUREKA:  
 1024 Physics and Engineering. 5. 37–46. [https://doi.org/10.21303/2461-](https://doi.org/10.21303/2461-4262.2019.00979)  
 1025 [4262.2019.00979](https://doi.org/10.21303/2461-4262.2019.00979)
- 1026 Tweddle, G.P., Froneman, P.W., 2017. Fish recruitment into a South African temporarily  
 1027 open/closed temperate estuary during three different hydrological mouth phases.  
 1028 African Journal of Marine Science. 39(2), 203–209.  
 1029 <https://doi.org/10.2989/1814232X.2017.1329168>

- 1030 Valle-Levinson, A., 2010. Contemporary Issues in Estuarine Physics. Cambridge  
1031 University Press. Cambridge. U.K. 326 pp.
- 1032 Vaz, L., Frankenbach, S., Serôdio, J., Dias, J.M., 2019. New insights about the primary  
1033 production dependence on abiotic factors: Ria de Aveiro case study. Ecological  
1034 Indicators. 106. 105555. <https://doi.org/10.1016/j.ecolind.2019.105555>
- 1035 Verocai, J., Nagy, G.J., Bidegain, M., 2016. Sea-level trends along freshwater and  
1036 seawater mixing in the Uruguayan Rio de la Plata estuary and Atlantic Ocean  
1037 coast. International Journal of Marine Science. 6(0). Article 0.  
1038 <https://www.aquapublisher.com/index.php/ijms/article/view/2282>
- 1039 Wenner, E.L., Knott, D.M., Barans, C.A., Wilde, S., Blanton, J.O., Amft, J., 2005. Key  
1040 factors influencing transport of white shrimp (*Litopenaeus setiferus*) post-larvae  
1041 into the Ossabaw Sound system. Georgia. USA. Fisheries Oceanography. 14(3),  
1042 175–194. <https://doi.org/10.1111/j.1365-2419.2005.00328.x>
- 1043 Wheeler, D.E., Epifanio, C.E., 1978. Behavioral response to hydrostatic pressure in  
1044 larvae of two species of xanthid crabs. Marine Biology. 46(2), 167–174.  
1045 <https://doi.org/10.1007/BF00391533>
- 1046 Whitfield, A.K., Potter, I.C., Neira, F.J., Houde, E.D., 2023. Modes of ingress by larvae  
1047 and juveniles of marine fishes into estuaries: From microtidal to macrotidal  
1048 systems. Fish and Fisheries, <https://doi.org/10.1111/faf.12745>  
1049  
1050